# Reference-free measurements of the 1s 2s 2p 2PO1=2;3=2! 1s2 2s 2S1=2 and 1s 2s 2p 4P5=2! 1s2 2s 2S1=2 transition energies and widths in lithiumlike sulfur and argon ions

J. Machado, Guojie Bian, Nancy Paul, M. Trassinelli, P. Amaro, M. Guerra, C.I. Szabo, A. Gumberidze, J.M. Isac, J. P. Santos, et al.

# Reference-free measurements of the $1s\ 2s\ 2p\ ^2P^{\rm O}_{1/2,3/2} \rightarrow 1s^2\ 2s\ ^2S_{1/2}$ and $1s\ 2s\ 2p\ ^4P_{5/2} \rightarrow 1s^2\ 2s\ ^2S_{1/2}$ transition energies and widths in lithiumlike sulfur and argon ions

J. Machado,[1,*] Guojie Bian,[2,3] Nancy Paul,[2,†] M. Trassinelli,[4,‡] P. Amaro,[1] M. Guerra,[1,§] C. I. Szabo,[5,¶] A. Gumberidze,[6,**] J.M. Isac,[2] J. P. Santos,[1,††] J.P. Desclaux,[7] and P. Indelicato[2,‡‡]

[1]*Laboratório de Instrumentação, Engenharia Biomédica e Física da Radiação (LIBPhys-UNL), Departamento de Física, Faculdade de Ciências e Tecnologia, FCT, Universidade Nova de Lisboa, 2829-516 Caparica, Portugal*

[2]*Laboratoire Kastler Brossel, Sorbonne Université, CNRS, ENS-PSL Research University, Collège de France, Case 74; 4, place Jussieu, F-75005 Paris, France*

[3]*Institute of Atomic and Molecular Physics, Sichuan University, Chengdu 610065, P.R. China*

[4]*Institut des NanoSciences de Paris, CNRS, Sorbonne Université ; 4, place Jussieu, F-75005 Paris, France*

[5]*Theiss Research, La Jolla, CA 92037, USA*

[6]*ExtreMe Matter Institute EMMI and Research Division, GSI Helmholtzzentrum für Schwerionenforschung, D-64291 Darmstadt, Germany*

[7]*15 Chemin du Billery, F-38360 Sassenage, France*

(Dated: November 12, 2019)

We have measured the widths and energies of the $1s2s2p\ ^2P_{1/2,3/2} \rightarrow 1s^22s\ ^2S_{1/2}$ transitions in lithiumlike sulfur and argon, as well as the energies of the forbidden $1s2s2p\ ^4P_{5/2} \rightarrow 1s^22s\ ^2S_{1/2}$ M2 transition in both elements. All measurements were performed with a double-flat crystal spectrometer without the use of any reference line. The transition energy measurements have accuracies ranging from 2.3 ppm to 6.4 ppm depending on the element and line intensity. The widths and the intensity ratios of the $1s2s2p\ ^2P_{1/2,3/2} \rightarrow 1s^22s\ ^2S_{1/2}$ lines have also been measured. These are the first reference-free measurements of transitions in core-excited lithiumlike ions, and have an accuracy comparable to the best relative measurements. We have also performed multi-configuration Dirac-Fock calculations of the widths, energies and intensity ratios. Extensive comparison between existing experimental results and theory is performed, and Bayesian techniques employed to extract the energy of the $1s\ 2p^2\ ^4P_{1/2} \rightarrow 1s^2\ 2p\ ^2P_{1/2}$ transition in sulfur and identify contaminant transitions.

PACS numbers: 34.80.Dp, 34.50.Fa, 34.10.+x

## I. INTRODUCTION

Since the beginning of the spectroscopy of highly charged ions (HCI), continuous improvement has been made in the accuracy of the measured transition energies across a broad range of elements. Measurements in HCI have extended the tests of the fundamental theory of the interaction between light and matter in bound systems, known as bound-state quantum electrodynamics (BSQED), to the strong-field regime. The most studied transitions are the $2p \rightarrow 1s$ transitions in hydrogenlike and heliumlike ions, and the $2p \rightarrow 2s$ transitions in heliumlike and lithiumlike ions (see [1] for a complete review). These studies are complementary to the progress made in high-accuracy measurements of transition energies in hydrogen [2–4]. Others fundamental quantities like the Landé $g$-factor in H-like ions such as carbon[5–8], oxygen[9], or silicon ($^{28}Si^{13+}$) [10, 11], and in Li-like ions like ($^{28}Si^{11+}$) [12], and the hyperfine structure have also been measured to provide tests of BSQED [1]. These advances in HCI spectroscopy have also provided important data for the diagnostic of astrophysical, laboratory and fusion plasmas.

Hydrogenlike ions have been studied across a wide range of elements up to uranium [1, 13]. A variety of techniques have been used, like beam foil spectroscopy, recoil ions, crystal spectroscopy on fast beams, or radiative electron capture at a storage ring electron cooler. More recently, very accurate, reference-free measurements of hydrogenlike ions [14, 15] have been reported using crystal spectrometers and highly-charged ion sources like electron-beam ion traps (EBIT). Their accuracy is of the order of a few parts per million (ppm), an order of magnitude improvement from previous measurements. The agreement between theory and experiment for one-electron ions is quite satisfactory (see for example [16]).

There have also been high-accuracy reference-free measurements of two-electron ions using both EBITs [15, 17] and electron cyclotron resonance ion sources (ECRIS)

* jfd.machado@fct.unl.pt
† npaul@lkb.upmc.fr
‡ trassinelli@insp.jussieu.fr
§ mguerra@fct.unl.pt
¶ csilla.szabo-foster@nist.gov
** A.Gumberidze@gsi.de
†† jps@fct.unl.pt
‡‡ Corresponding Author: paul.indelicato@lkb.upmc.fr

[18, 19] . Agreement between measurements in heliumlike ions and QED calculations [20] is also excellent (see Refs. [1, 19] for a detailed review of available measurements and comparison with theory). For three-electron ions there are very accurate measurements and calculations for the $1s^22p\ ^2P_J \rightarrow 1s^22s\ ^2S_{1/2}$ transitions, for elements up to very heavy ones like lead, bismuth, thorium and uranium [21–28] using both EBITs and accelerators. For these systems, an overall good agreement is found between all the available experiments and the most advanced calculations [1, 29–32].

The situation is very different for transitions in lithiumlike ions with a core-excited initial level, like the $1s2s2p\ ^2P_J$ level, often observed as satellites of the heliumlike transitions. A number of measurements have been made, but most of them are relative, and not very accurate. Considering just the measurements for $Z \geq 10$ and of the transitions labeled q ($1s2s2p\ ^2P^{\rm O}_{3/2} \rightarrow 1s^22s\ ^2S_{1/2}$) and r ($1s2s2p\ ^2P^{\rm O}_{1/2} \rightarrow 1s^22s\ ^2S_{1/2}$) by Gabriel [33], we can cite in chronological order several experiments performed for $11 \leq Z \leq 17$ and K, Ti and V [34], for Si [35], Ti [36], Ar [37], Sc, V, Cr and Mn [38], Ni [39], V [40], Ca [41], Co [42], Sc [43], Fe [44], Ne [45], Ar [46, 47], Fe [48], Ar [49], Fe [50], S, Cl and Ar [51], and Ca [52]. These measurements were performed using laser-generated plasmas [34], beam-foil spectroscopy and tokamaks. To our knowledge, there is only one measurement for $Z > 28$, performed on the Livermore EBIT for the q line of praseodymium ($Z = 59$) [53]. For the $1s2s2p\ ^4P_{5/2} \rightarrow 1s^22s\ ^2S_{1/2}$ transition, its energy has been measured only in Ar [47, 54].

In 2013, Schlesser *et al.* [51] reported high-accuracy (around 1 ppm) measurements of the $1s2s2p\ ^2P^{\rm O}_J \rightarrow 1s^22s\ ^2S_{1/2}$ transition in lithiumlike sulfur, chlorine and argon using a spherical-crystal spectrometer and an ECRIS. These measurements are relative to the theoretical predictions of the M1 line energy by Artemyev *et al.* [20]. To our knowledge, the only available reference-free measurement of a transition from a core-excited, auto ionizing level, is that of the $1s2s^22p\ ^1P_1 \rightarrow 1s^22s^2\ ^1S_0$ transition in Be-like argon [19]. The very accurate measurements of several core-excited lines performed using an EBIT and the PETRA III synchrotron radiation facility use $K$-edges of several elements (Mn, Fe, Co, Ni, and Cu) for calibration [50].

The $1s2s2p\ ^2P^{\rm O}_J$ levels can decay by either radiative transitions to a variety of singly and doubly excited levels, or by the Auger effect. Yet there is a single Auger transition to the ground state of the corresponding He-like ion. They are thus a good test case for testing the Auger decay theory. Contrastingly, in core-excited neutral atoms there can be tens of Auger decay channels. Even for the case of the $1s2s^22p\ ^1P_1 \rightarrow 1s^22s^2\ ^1S_0$ transition in Be-like ions there are still three possible Auger transitions. Another feature of these lithiumlike ion core-excited states is that, since the initial level is degenerate with a continuum, it is shifted (the so-called Auger shift) [55–58].

Because of the theoretical interest in a better understanding of the QED, correlation and Auger shift contributions to the initial level energy, we have performed in the present work reference-free measurements of the $1s2s2p\ ^2P^{\rm O}_J \rightarrow 1s^22s\ ^2S_{1/2}$ and of the $1s2s2p\ ^4P_{5/2} \rightarrow 1s^22s\ ^2S_{1/2}$ transition energies in sulfur and argon with accuracies of a few ppm. We have also measured the widths of the lines. To our knowledge the widths of the r and q transitions have been measured only for iron [50].

The experimental method used to make these measurements has been described in Ref. [59]. This method has already been used to measure with few ppm accuracy the $1s2s\ ^3S_1 \rightarrow 1s^2\ ^1S_0$ M1 line [18] and the $1s2p^1P_1 \rightarrow 1s^2\ ^1S_0$ transition [19] energies in He-like argon ions. It was also used to measure the $1s2s^22p^1P_1 \rightarrow 1s^22s^2\ ^1S_0$ transition energy and width in Be-like argon ions [19]. Accurate calculations of the transition energies and widths performed using the Multi-Configuration Dirac-Fock (MCDF) method are also presented.

The article is organised as follows. In Sec. II we briefly describe the experimental setup used in this work and provide a detailed description of the analysis method, which allows us to obtain the energies and widths with their uncertainties. A brief description of the calculations of transition energies and widths is given in Sec. III. Sec. IV presents a detailed discussion of the experimental results and comparison with theory for both S and Ar lines. The conclusions are provided in Sec. V.

## II. EXPERIMENTAL METHOD AND DATA ANALYSIS

### A. Description of the experiment

The detailed description of the experimental method may be found in Refs. [18, 19, 59]. Here we only recall the main features of the experiment. A double-flat crystal spectrometer is attached to an electron-cyclotron resonance ion source. The optical axis of the spectrometer is aligned with the ECRIS axis. The plasma in the source has a diameter of ≈30 mm. The plasma is seen from the spectrometer through a copper tube of an inner diameter of 12 mm. The microwave power to create and maintain the plasma was around 300 W. For measuring the transition energies in argon, a mixture of argon gas and oxygen was injected into the source. For sulfur, $SF_6$ gas and oxygen were used. In the argon measurement, we used the same gas-filled proportional counter as in Ref. [59]. In the sulfur measurement we used a large area avalanche photodiode (LAAPD). The vacuum of the source and the one of the spectrometer were separated by a thiner 50 µm thick Be window. The LAAPD is mounted on a copper support cooled to ≈ − 10 °C using a mixture of ethanol and water to reduce thermal electronic noise. Several blocks of copper, cooled in the same way, were used at different hot spots inside the spectrometer to stabilize the temperature. The spectrometer is under vacuum to avoid

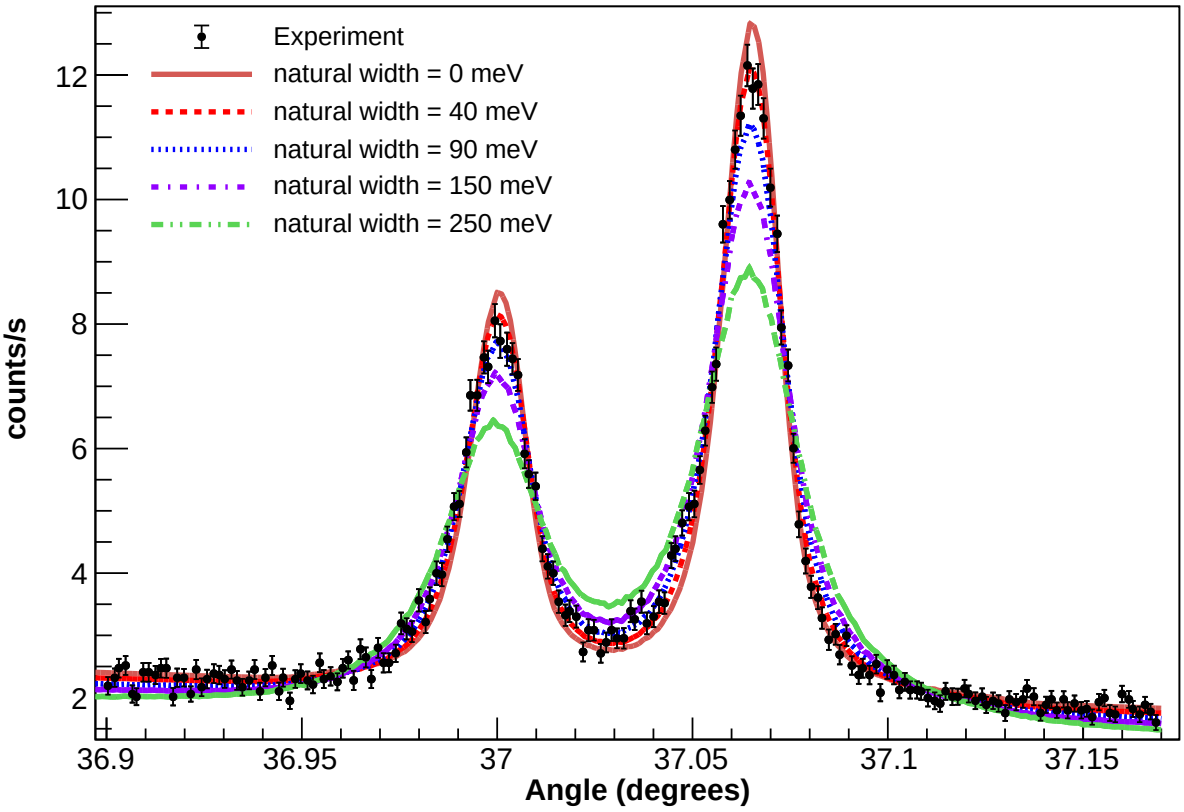


FIG. 1: (Color online) Example of fits to a dispersive spectrum of the $1s\ 2s\ 2p\ ^2P_J \rightarrow 1s^2\ 2s\ ^2S_{1/2}$, $J = 1/2, 3/2$ transitions in lithiumlike sulfur. A subset of the simulation spectra with Lorentzian widths values $\Gamma_L = 0$ meV, 40 meV, 90 meV, 150 meV and 250 meV is shown. The error bar for each experimental point is $\sqrt{n}/t$, where $n$ is the number of counts and $t$ the measurement time of the bin.

absorption of the low-energy x rays by air. The stepping motors used by the rotation table are cooled to avoid heat drift. Heating resistors are mounted on the backs of the crystals and connected to a temperature controller with a proportional–integral–derivative controller (PID) which is used to stabilize the crystal temperatures.

Between the argon and the sulfur experiment the ECRIS and the spectrometer had to be moved and fully realigned using the procedure described in Ref. [59] because of construction work in the original location. Checks were performed on the intense Be-like Argon line $1s2s^22p\ ^1P_1 \rightarrow 1s^22s^2\ ^1S_0$ line, and the results were found to be in agreement with our earlier measurement [19].

During the work on argon, the vacuum of the source and the one of the spectrometer were separated by a 125 µm-thick Be window. The polarization electrode, which is used to apply a voltage to the plasma to optimize performances, and through which the x-rays detected by the DCS are passing, had an inner diameter of 12 mm for a length of 300 mm. In the setup used for sulfur, after moving the source, we used a slightly different arrangement with a polarisation electrode of the same length, but an inner diameter of 8 mm, identical to the initial design of the SuperNanogan ECRIS we are using, and a 50 µm thick Be window. The thicker Be window has a transmission of 39 % at the x-ray energy of lithiumlike sulfur and 64 % at the x-ray energy of lithiumlike argon [60]. The thiner one has a transmission of 68 % and 88 % respectively, partially compensating for the transmission loss due to the smaller electrode diameter.

During the measurements on sulfur, we found out that the source operations were more stable than with argon before, which allowed to obtain more statistics in the sulfur spectra.

### B. Data analysis

The data analysis was performed in a similar way as in Ref. [19]. Yet, in the present case, the dispersive spectra have two lines that are not completely resolved. We thus

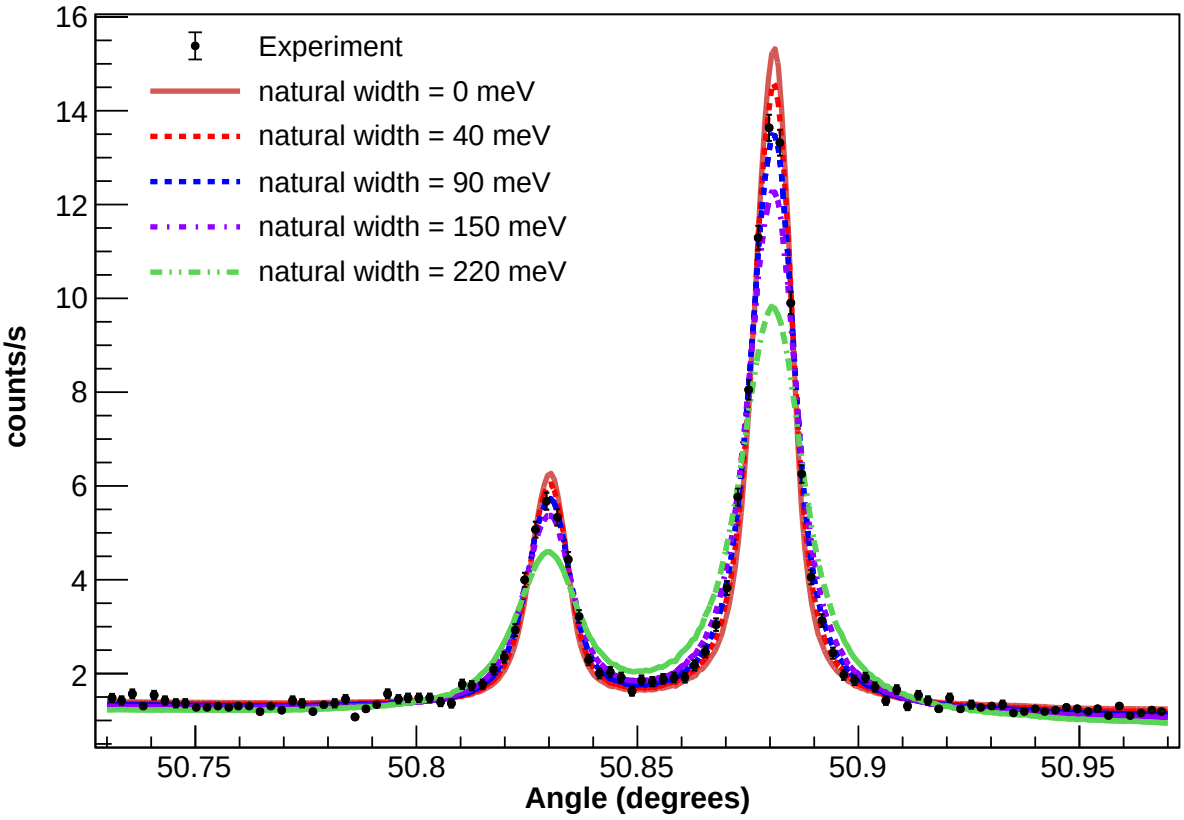


FIG. 2: (Color online) Example of fits to a dispersive spectrum of the $1s\ 2s\ 2p\ ^2P_J \rightarrow 1s^2\ 2s\ ^2S_{1/2}$, $J = 1/2, 3/2$ transitions in lithiumlike argon. A subset of the simulated spectra with Lorentzian widths values $\Gamma_L = 0\,\text{meV}$, 40 meV, 90 meV, 150 meV and 250 meV is shown. The error bar for each experimental point is $\sqrt{n}/t$, where $n$ is the number of counts and $t$ the measurement time of the bin.

had to modify the analysis method to obtain the experimental line widths and energies. We first describe the method for obtaining the line widths and then how we derived the line energies.

### 1. *Line widths*

The determination of the line widths has been performed with the following procedure:

- A set of simulations is performed using the *ab initio* code developed in Ref. [59] with theoretical energies $E_0$, Gaussian Doppler broadening for sulfur of $\Gamma_G^{\text{Exp.}} = 91.7(74)\,\text{meV}$, which was obtained by fitting experimental spectra of the He-like M1 line, as was done for argon in Ref. [18]. This broadening corresponds to the depth of the trapping well created by the space charge of the electrons in the ECRIS plasma. This depth is around $\approx$0.2 V [61, 62]. For Argon we use $\Gamma_G^{\text{Exp.}} = 80.5(46)\,\text{meV}$, the value obtained in [18]. The Lorentzian widths used in the simulation $\Gamma_L^i$ have been taken in the range from 0 meV to 400 meV. A set of 25 simulations was performed and the crystal temperatures used in these simulations was $T_{\text{Ref.}} = 22.5\,^\circ\text{C}$;
- The spectra from the simulation are interpolated using splines to obtain a set of parametrized, continuous functions $S_{E_0,\Gamma_L^i,\Gamma_G^{\text{Exp.}},T_{\text{Exp.}}}(\theta - \theta_0)$;
- Each experimental dispersive spectrum is fitted with all the possible combinations of two of the interpolated functions described above according to

$$\begin{aligned} &I(\theta-\theta_0^1,\theta-\theta_0^2,I_{\max}^1,I_{\max}^2,a^1,a^2,b^1,b^2) = \\ &I_{\max}^1 S_{E_0,\Gamma_L^1,\Gamma_G^{\text{Exp.}},T_{\text{Exp.}}}(\theta-\theta_0^1) \\ &+ I_{\max}^2 S_{E_0,\Gamma_L^2,\Gamma_G^{\text{Exp.}},T_{\text{Exp.}}}(\theta-\theta_0^2) + a + b\theta, \end{aligned} \tag{1}$$

where the superscripts 1 and 2 represent the two lines in the spectrum, $I_{max}^1$ and $I_{max}^2$ the line intensities, $\theta$ the second crystal angle, $\theta_0^1$ and $\theta_0^2$ the

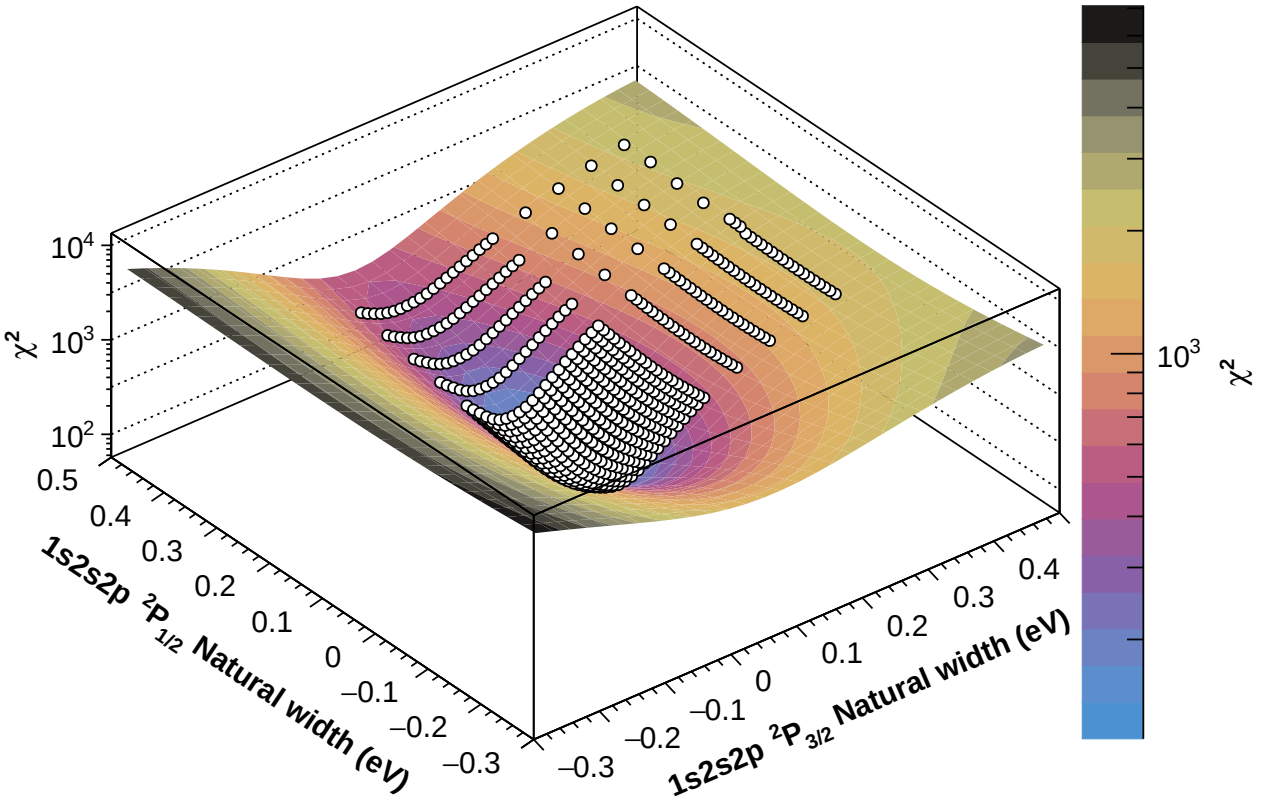


FIG. 3: (Color online) Fit to the set of points $[\chi^2, \Gamma_L^1, \Gamma_L^2]$ for argon using Eq. (2). The $\chi^2$ values are obtained from the fits shown on Fig. 2 for the respective combination of Lorentzian widths $[\Gamma_L^1, \Gamma_L^2]$. From the optimized fit function by $\chi^2$ minimization the pair of optimum Lorentzian widths $[\Gamma_L^1, \Gamma_L^2]$ is obtained by getting the minimum of the function. The $z$ coordinate $(\chi^2)$ is shown in log scale. Each white dot corresponds to one simulation. In this example, the minimum $\chi^2 = 101.26$ has been obtained, corresponding to a reduced $\chi_r^2 = 1.08$. The total number of degrees of freedom is 94 (100 points minus 6 free coefficients in the fitted function).

offset angles between the experimental and simulated spectra for each line, $a$ the background intensity and $b$ the background slope. The parameters $I_{max}^j$, $\theta_0^j$, $a$ and $b$ are adjusted to minimize $\chi^2\left(\Gamma_L^1, \Gamma_L^2\right)$. The combination of the different simulated Lorentzian widths corresponds to a total of 625 fits of each experimental dispersive spectra. Examples of a fitted spectrum with a subset of different Lorentzian widths is shown in Figs. 1 for sulfur and 2 for argon; All

- The $\chi^2$ is evaluated for each fit. The bidimensional function

$$\begin{aligned}\chi^2(\Gamma_L^1, \Gamma_L^2) =& a + b\Gamma_L^1 + c\Gamma_L^2 + d\Gamma_L^1\Gamma_L^2 \\ &+ e(\Gamma_L^1)^2 + f(\Gamma_L^2) + g(\Gamma_L^1)^3 \\ &+ h(\Gamma_L^2)^3\end{aligned} \qquad (2)$$

is fitted to the set of points $[\chi^2, \Gamma_L^1, \Gamma_L^2]$, where $a, b, c, d, e, f, g$ and $h$ are adjustable parameters to the set of points obtained. An example of the bidimensional fit to the set of points $[\chi^2, \Gamma_L^1, \Gamma_L^2]$ for one argon spectrum is presented in Fig. 3;

- The minimum of the bidimensional fit function is used to find the best pair of widths $[\Gamma_{L\,\mathrm{opt.}}^1, \Gamma_{L\,\mathrm{opt.}}^2]$ for the $1s\ 2s\ 2p\ ^2P_J \rightarrow 1s^2\ 2s\ ^2S_{1/2}$ doublet;

- The 68% error bars, $\delta\Gamma_{L\,\mathrm{opt.}}^1$ and $\delta\Gamma_{L\,\mathrm{opt.}}^2$, are extracted for each obtained natural width $([\Gamma_{L\,\mathrm{opt.}}^1, \Gamma_{L\,\mathrm{opt.}}^2])$, by finding the values for which [63]

$$\chi^2\left(\Gamma_{L\,\mathrm{opt.}}^{1,2} \pm \delta\Gamma_{L\,\mathrm{opt.}}^{1,2}\right) = \chi^2\left(\Gamma_{L\,\mathrm{opt.}}^{1,2}\right) + 1. \qquad (3)$$

In Fig. 4 a zoom in around the minimum value of the $\chi^2$ grid of Fig. 3 is presented. The colored

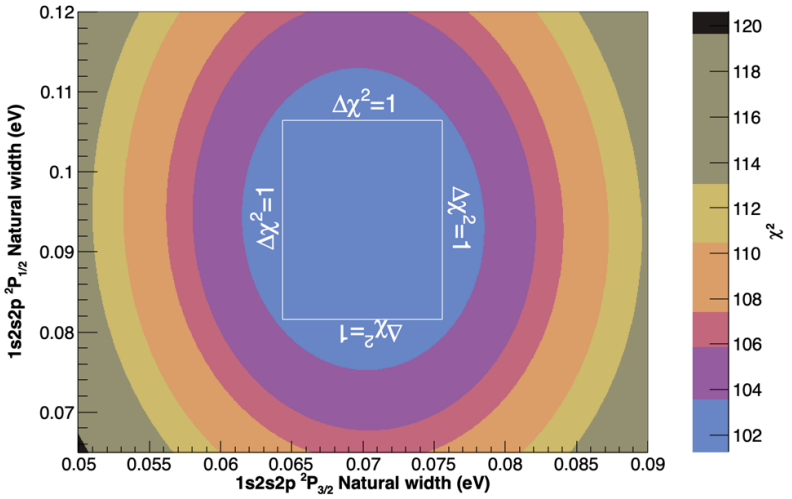


FIG. 4: (Color online) Zoom in around the minimum value of the $\chi^2$ grid of Fig. 3. The colored contours represent the $n\sigma$ confidence intervals for the two variables $[\Gamma^1_{L\,\mathrm{opt.}}, \Gamma^2_{L\,\mathrm{opt.}}]$ around the minimum $\chi^2$ value, for $n = 1, 2, 3, \cdots$. The 68 % confidence interval given by Eq. (3), where the interval is obtained for each natural width, is shown on the plot by the $\Delta\chi^2 = 1$ white lines.

contours shown in Fig. 4 represent the confidence intervals of the $\chi^2$ grid for the two widths values $[\Gamma^1_{L\,\mathrm{opt.}}, \Gamma^2_{L\,\mathrm{opt.}}]$. Each different contour is the $n\sigma$ confidence intervals, for $n = 1, 2, 3, \cdots$. The individual $1\sigma$ confidence interval for each variable ($\delta\Gamma^1_{L\,\mathrm{opt.}}$ and $\delta\Gamma^2_{L\,\mathrm{opt.}}$) is represented by the interval between the $\Delta\chi^2 = 1$ lines above the minimum $\chi^2$ value, which are illustrated by the white lines in Fig. 4;

- Finally, a weighted average is performed of each set of ($\Gamma^1_{L\,\mathrm{opt.}}$) and ($\Gamma^2_{L\,\mathrm{opt.}}$), the pair of widths for each recorded spectrum, including uncertainties. The mean value and the $\pm\sigma$ interval for the pair of widths of the $1s\ 2s\ 2p\ ^2P_J \rightarrow 1s^2\ 2s\ ^2S_{1/2}$ doublet are presented on Figs. 5 and 6.

For the $1s\ 2s\ 2p\ ^4P_{5/2} \rightarrow 1s^2\ 2s\ ^2S_{1/2}$ transition, the procedure is different. The line is a small, well separated satellite of the $1s\ 2s^2\ 2p\ ^1P_1 \rightarrow 1s^2\ 2s^2\ ^1S_0$ transition in berylliumlike sulfur or argon, as shown in Figs. 7 and 8. The natural width of the line is very small as shown in Sec. III. Thus only the Doppler width is used as the line width. This was checked by fitting a simulated profile convolved with a Gaussian. The width of the Gaussian was varied and the $\chi^2$ evaluated. The value found is consistent, within the uncertainties, with the Doppler width obtained from the heliumlike M1 transition.

*2. Transition energies of the $1s\ 2s\ 2p\ ^2P_J \rightarrow 1s^2\ 2s\ ^2S_{1/2}$ doublet*

For the energy analysis, the method is similar to the one described in Ref. [19]. The difference between the two methods lies in the interpolated functions (constructed by the simulation output), which are fitted to the experimental spectra. For the non-dispersive spectrum there is no difference, since there is only one peak for both transitions. Yet for the dispersive spectra, which contains two lines, we calculate fit functions using the two values of the natural widths obtained in the procedure above. We then perform a spline interpolation of the simulation, using Eq. (1). The non-dispersive spectra obtained from the simulations for both transitions are identical, as they only depend on the angular settings of the spectrometer, which are kept fixed for all simulations. The spline interpolation in this case is constructed using

$$I(\theta - \theta_0, I_{\max}, a, b) = I_{\max} S(\theta - \theta_0) + a + b\theta. \quad (4)$$

We do a set of simulations, using five different energies $E_k = E_{\mathrm{theo.}} + k\Delta E$ with $\Delta E = 0.01\,\mathrm{eV}$, $k \in \{-2, -1, 0, 1, 2\}$ and 10 different temperatures $T_l$ ranging from 20 °C to 30 °C for each line. For each simulation, we get as output a dispersive mode (DM) and non-dispersive mode (NDM) spectra. We obtain the offset angles $\theta^1_{0\,\mathrm{DM}}$ and $\theta^2_{0\,\mathrm{DM}}$ from the fits to the DM (see Eq. (1)) and $\theta_{0\,\mathrm{NDM}}$ from the NDM peaks (see Eq. (4)) and thus there is a single value for the NDM offset angle. The difference of the DM and NDM offset angle differences between an experimental spectrum and a simulation are obtained

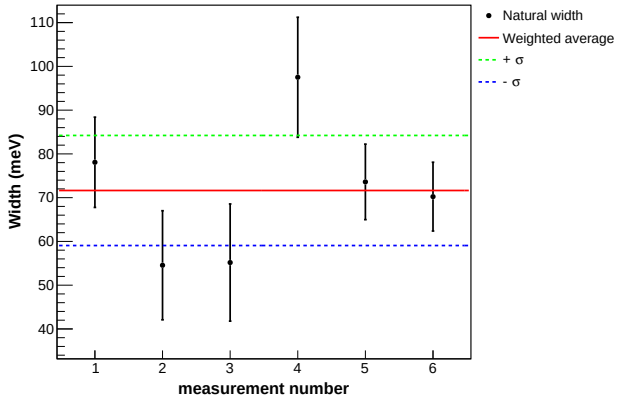


(a) $1s\ 2s\ 2p\ ^2P_{1/2} \rightarrow 1s^2\ 2s\ ^2S_{1/2}$.

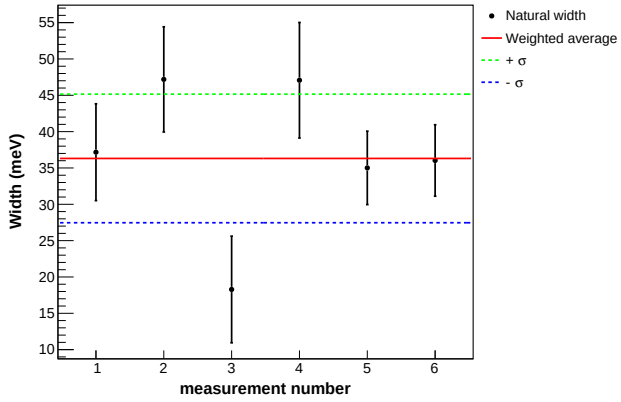


(b) $1s\ 2s\ 2p\ ^2P_{3/2} \rightarrow 1s^2\ 2s\ ^2S_{1/2}$.

FIG. 5: (Color online) Natural widths of all spectra recorded during the measurement of the $1s\ 2s\ 2p\ ^2P_J \rightarrow 1s^2\ 2s\ ^2S_{1/2}$, $J = 1/2,\ 3/2$ Li-like sulfur transitions. The weighted average and the 68% confidence interval ($\pm 1\sigma$) are also shown.

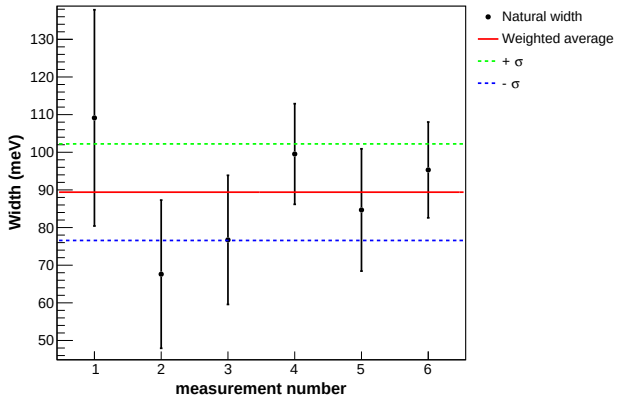


(a) $1s\ 2s\ 2p\ ^2P_{1/2} \rightarrow 1s^2\ 2s\ ^2S_{1/2}$.

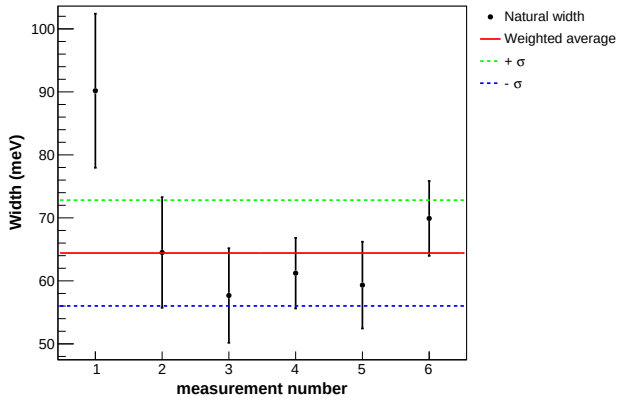


(b) $1s\ 2s\ 2p\ ^2P_{3/2} \rightarrow 1s^2\ 2s\ ^2S_{1/2}$.

FIG. 6: (Color online) Natural widths of all spectra recorded during the measurement of the $1s\ 2s\ 2p\ ^2P_J \rightarrow 1s^2\ 2s\ ^2S_{1/2}$, $J = 1/2,\ 3/2$ Li-like argon transitions. The weighted average and the 68% confidence interval ($\pm 1\sigma$) are also shown.

from

$$\Delta\theta^{j,k,l,n}_{\text{Exp.}-\text{Simul.}} = (\theta^{n}_{\text{Exp.DM}} - \theta^{n,j}_{\text{Exp.NDM}}) - (\theta^{j,k,l}_{\text{Simul.DM}} - \theta^{k,l}_{\text{Simul.NDM}}) \quad (5)$$

with $j = 1,\ 2$ representing each transition in the doublet, $k, l$ the energy and temperature used in the simulation, and $n$ the number of the daily measurements. If the energy and temperature used in the simulations were identical to the experimental values during the data acquisition, this difference of offset angle differences should be zero. For each peak, the bidimensional function

$$\Delta\theta_{\text{Exp.}-\text{Simul.}}(E,T) = p + qE + rE^2 + sET + uT + vT^2, \quad (6)$$

where $p, q, r, s, u$ and $v$ are adjustable parameters, is fitted to the set of points $\left[E_k, T_l, \Delta\theta^{j,k,l,n}_{\text{Exp.}-\text{Simul.}}\right]$. An example of the bidimensional fit function for each Li-like transition is presented in Fig. 9.

From the two bidimensional fit functions, the experimental line energy $E^n_{\text{Exp.}}$ for spectrum pair number $n$, is obtained from the relation $\Delta\theta_{\text{Exp.}-\text{Simul.}}(E^n_{\text{Exp.}}, T_{\text{Exp.}}) = 0$, where $T_{\text{Exp.}}$ indicates the measured average temperature on the second crystal. When all experimental energy values for each pair of dispersive and non-dispersive spectra have been obtained, a weighted average is performed and the final value of the energy is obtained with the respective statistical uncertainty. The values obtained for each pair of dispersive and non-dispersive spectra for both Li-like lines are presented in Fig. 10 for sulfur and

TABLE I: Contributions to the systematic uncertainties for sulfur. All energies are given in eV.

| Contribution | Value (eV) |
|---|---|
| Index of refraction | 0.00055 |
| Angle encoder error (0.2″) | 0.00171 |
| Temperature (0.5 °C) | 0.00312 |
| Energy—wavelength correction | 0.00006 |
| Lattice spacing error | 0.00010 |
| Thermal expansion | 0.00015 |
| Energy dependance of the width | 0.00031 |
| x-ray polarization | 0.00513 |
| x-ray source size (6 mm to 12 mm) | 0.00462 |
| Crystal tilts (±0.01 °C for each crystal) | 0.00085 |
| Vertical divergence (±0.01 mm) | 0.00102 |
| Form factors | 0.00212 |
| Total | 0.00819 |

Fig. 11 for argon. The weighted average is represented by the solid red line and the dashed red and blue lines represent the $+\sigma$ and $-\sigma$, respectively. The error bar at each point corresponds to the statistical uncertainty of obtaining the energy value from the bidimensional fit function, presented in Fig. 9 for the case of argon as an example, quadratically combined with the uncertainties due to the temperature and angle measurements. Every pair of points on both plots of Figs. 10 and 11 corresponds to one day of data taking.

The systematic uncertainty is obtained in the same way as described in Refs. [18, 19, 59]. The resulting values for sulfur are presented in Table I.

#### 3. *Transition energies of the* $1s\ 2s\ 2p\ ^4P_{5/2} \rightarrow 1s^2\ 2s\ ^2S_{1/2}$ *transition and adjacent lines*

Using the method described above, we have obtained the energy of the $1s\ 2s\ 2p\ ^4P_{5/2} \rightarrow 1s^2\ 2s\ ^2S_{1/2}$ transition in both sulfur and argon. Yet for sulfur, we find evidence in the residuals of the presence of a third peak, as shown in Fig. 12. In order to to certify its existence, and obtain its energy, we used advanced Bayesian techniques, as implemented in the NestedFit analysis package described in [64]. This package is based on the methods developed in Refs. [65–68]. With this technique we find overwhelming evidence of the presence of a third peak between the $1s\ 2s\ 2p\ ^4P_{5/2} \rightarrow 1s^2\ 2s\ ^2S_{1/2}$ and the $1s\ 2s^2\ 2p\ ^1P_1 \rightarrow 1s^2\ 2s^2\ ^1S_0$ transitions, with a gain in ln(evidence) of 242.1(3), corresponding to a $p$-factor of $1.07 \times 10^{-108}$, essentially 0. The difference in the fits and residuals when including this peak are shown in Fig. 12. The probability distribution of the centroid of this third peak is shown in Fig. 13. For Argon, we do not find statistical evidence of the presence of such a peak. The identification of this peak will be discussed in Sec. IV B.

## III. THEORETICAL EVALUATION OF THE ENERGIES AND WIDTHS OF THE MEASURED TRANSITIONS

We have evaluated the energies of the $1s\ 2s\ 2p\ ^2P_{1/2} \rightarrow 1s^2\ 2s\ ^2S_{1/2}$, $1s\ 2s\ 2p\ ^2P_{3/2} \rightarrow 1s^2\ 2s\ ^2S_{1/2}$ and $1s\ 2s\ 2p\ ^4P_{5/2} \rightarrow 1s^2\ 2s\ ^2S_{1/2}$ transitions in sulfur and argon using the code (MCDFGME), developed by Desclaux and Indelicato [69–72]. This code has been recently modified to be able to calculate the self-energy screening correction following the model operator approach recently developed in Refs [73, 74], in the same way as our recent work on Be-like argon[19]. We used the 2018 version of the code, which takes into account the most-recent two-loop self-energy correction calculations [75], although their effect is very small here. The full description of the method and the code can be found in Refs. [69, 76–78]. The code also evaluates the normal and specific mass shifts, following [79–81], as described in [82, 83]. All calculations were done for a finite nucleus modeled as a uniformly charged sphere. The atomic masses are taken from the tables in Ref. [84] and the nuclear radii from [85, 86], respectively.

The main advantage of the MCDF approach is the ability to include a large amount of electronic correlation by taking into account a limited number of configurations [87–89]. Here we have included all singly, doubly and triply excited configurations up to $5g$ orbitals. The calculation is rather difficult for the excited state, when the $1s2s$ core acquires a $^1S_0$ component. In this case, the off-diagonal Lagrange multiplier that is used to maintain the orthogonality between the two orbitals tends to become very small and the $2s$ orbitals tends to become identical to the $1s$. We thus added the ground state configuration $1s^22s$ for these cases, which prevents this from occuring.

One-electron radiative corrections are exact QED values. The one-electron self-energy is taken from the work of Mohr and co-workers [90–94], and corrected for finite nuclear size [95]. The self-energy screening and vacuum polarization are calculated following [55, 57, 70, 71, 96]. Here we compare the self-energy screening obtained using the Welton approximation [70, 71] and the approach from Ref. [73, 74]. The two-loop self-energy is taken from [75, 97–103]. The SEVP and S(VP)E corrections are obtained from Ref. [101]. The Källèn and Sabry potential is also included, as described in Ref. [104]. The full Breit interaction and the Uehling potential are included in the self-consistent field process, which provides higher-order corrections. Projection operators have been included [78] to avoid coupling with the negative energy continuum.

The details of the different contributions for sulfur are presented in Table II and for argon in Table III.

Radiative transition probabilities are evaluated using the method described in Ref. [105]. The orbitals contributing to the wave function were fully relaxed, and the resulting non-orthogonality between initial and final wave functions fully taken into account, following [106, 107].

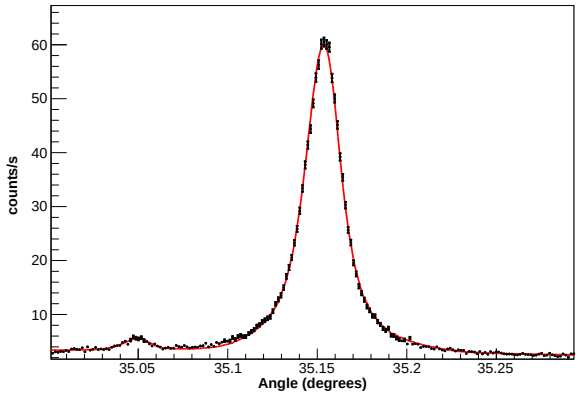


(a) $1s\ 2s\ 2p\ ^4P_{5/2} \rightarrow 1s^2\ 2s\ ^2S_{1/2}$ and $1s\ 2s^2\ 2p\ ^1P_1 \rightarrow 1s^2\ 2s^2\ ^1S_0$.

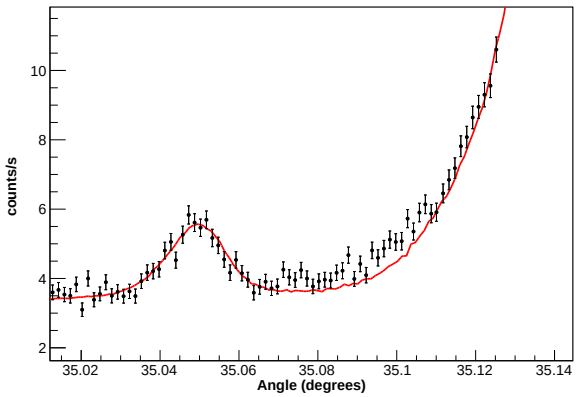


(b) Zoom on $1s\ 2s\ 2p\ ^4P_{5/2} \rightarrow 1s^2\ 2s\ ^2S_{1/2}$.

FIG. 7: (Color online) Spectrum of the $1s\ 2s\ 2p\ ^4P_{5/2} \rightarrow 1s^2\ 2s\ ^2S_{1/2}$ and $1s\ 2s^2\ 2p\ ^1P_1 \rightarrow 1s^2\ 2s^2\ ^1S_0$ transitions in Li-like and Be-like sulfur. The best fit corresponds to a Lorentzian width of 0 meV for the $1s\ 2s\ 2p\ ^4P_{5/2} \rightarrow 1s^2\ 2s\ ^2S_{1/2}$ transition. See text and Ref. [18] for more details.

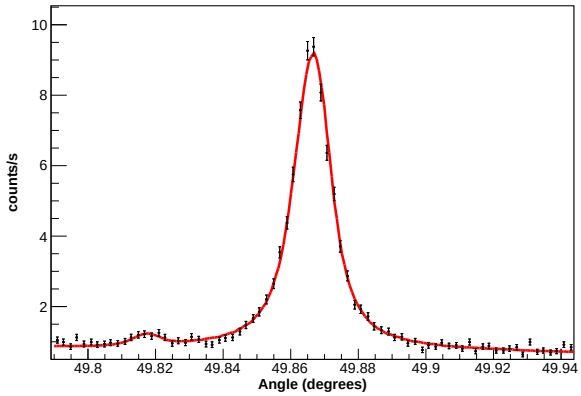


(a) $1s\ 2s\ 2p\ ^4P_{5/2} \rightarrow 1s^2\ 2s\ ^2S_{1/2}$ and $1s\ 2s^2\ 2p\ ^1P_1 \rightarrow 1s^2\ 2s^2\ ^1S_0$.

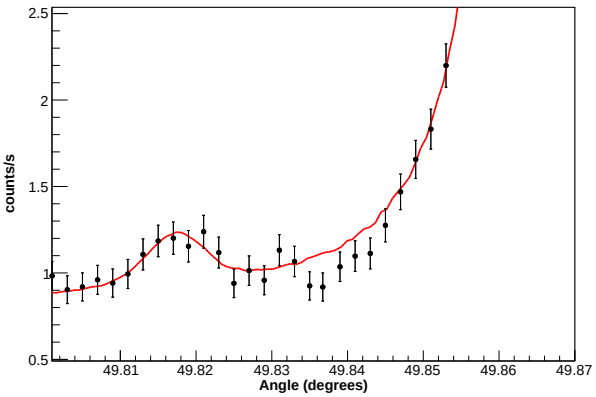


(b) Zoom on $1s\ 2s\ 2p\ ^4P_{5/2} \rightarrow 1s^2\ 2s\ ^2S_{1/2}$.

FIG. 8: (Color online) Spectrum of the $1s\ 2s\ 2p\ ^4P_{5/2} \rightarrow 1s^2\ 2s\ ^2S_{1/2}$ and $1s\ 2s^2\ 2p\ ^1P_1 \rightarrow 1s^2\ 2s^2\ ^1S_0$ transitions in Li-like and Be-like argon. The best fit corresponds to a Lorentzian width of 0 meV for the $1s\ 2s\ 2p\ ^4P_{5/2} \rightarrow 1s^2\ 2s\ ^2S_{1/2}$ transition. See text and Ref. [18] for more details.

The radiative transition rates to other levels have also been evaluated. We thus take into account in the total width, all transitions of the type $1s\ 2s\ 2p\ ^2P_J \rightarrow 1s^2\ nlj$, with $n \leq 7$, $l \leq n$ and all possible values of $j$.

The Auger widths of the $1s\ \ 2s\ \ 2p\ \ ^2P_J$ and $1s\ \ 2s\ \ 2p\ \ ^4P_{5/2}$ levels are calculated using the MCDFGME code, as described in Ref. [108]: the initial and final state orbitals are fully relaxed, we use final-state channel mixing and take into account the non-orthogonality between the fully relaxed orbitals in the initial and final state.

The results for the radiative and Auger lifetimes, and fluorescence yields for sulfur and argon are presented in Tables IV. and V respectively.

The transition energies and rates have also been evaluated for comparison with the "flexible atomic code" (FAC), widely used in plasma physics [109].

## IV. RESULTS AND DISCUSSION

### A. Values of the widths

The experimental widths obtained using the method explained in Sec. II B 1 are presented for S in Fig. 5 and for Ar in Fig. 6. The values are given in Table VI, and

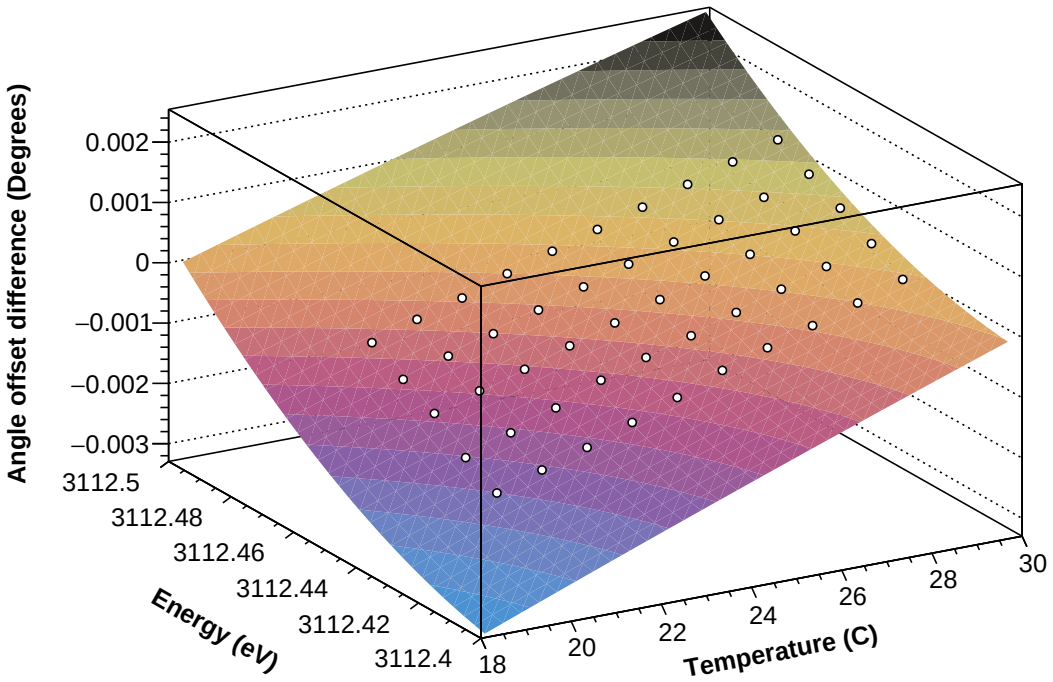


(a) $1s\ 2s\ 2p\ ^2P_{1/2} \rightarrow 1s^2\ 2s\ ^2S_{1/2}$.

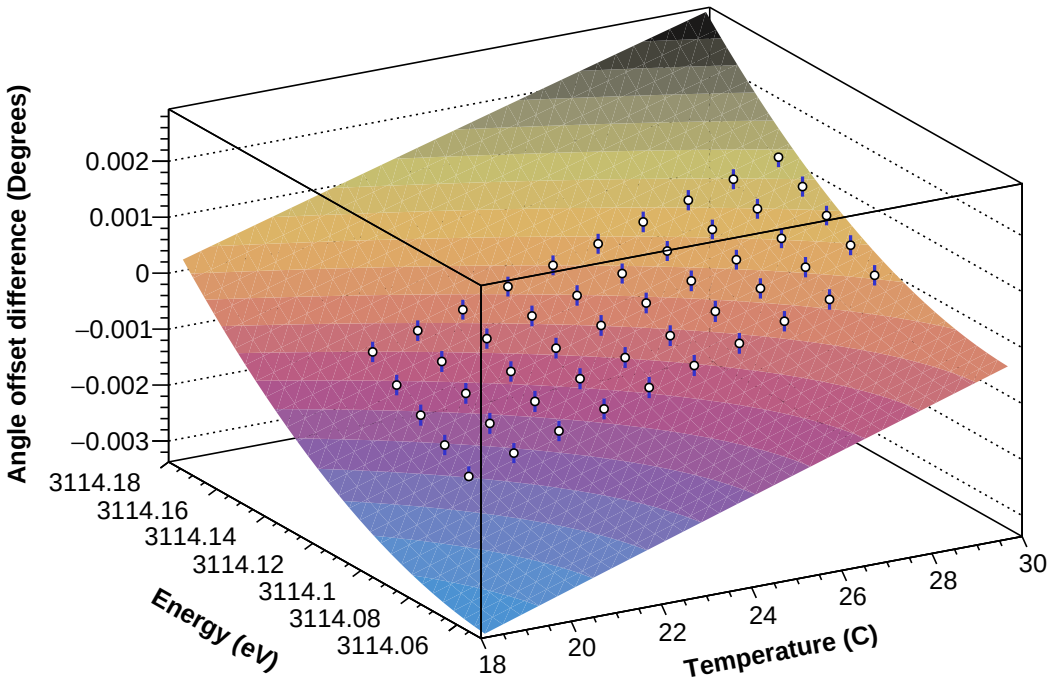


(b) $1s\ 2s\ 2p\ ^2P_{3/2} \rightarrow 1s^2\ 2s\ ^2S_{1/2}$.

FIG. 9: (Color online) Example of the fit with the bidimensional function (Eq. (6)) to the set of data $\left[E_k, T_l, \Delta\theta^{k,l}_{\text{Exp.}-\text{Simul.}}\right]$ for the two measured Li-like transitions in argon, with the offset $\Delta\theta^{n,k,l}_{\text{Exp.}-\text{Simul.}}$ obtained by fitting both dispersive and non-dispersive spectra. The error bar at each point is calculated from the quadratic sum of the standard errors $\delta\theta$ of the offset $\theta$ fit parameter from the dispersive and non-dispersive spectra.

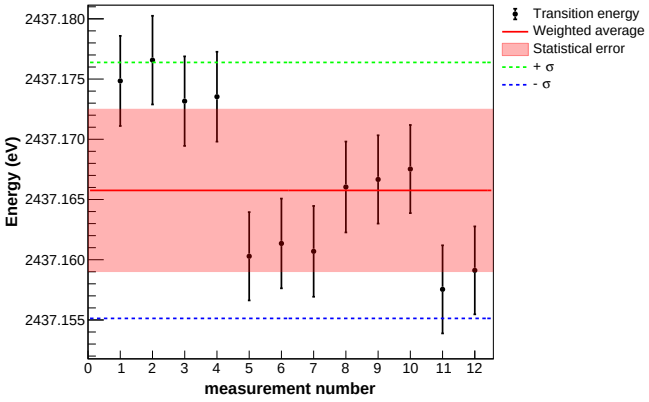


(a) $1s\ 2s\ 2p\ ^2P_{1/2} \rightarrow 1s^2\ 2s\ ^2S_{1/2}$.

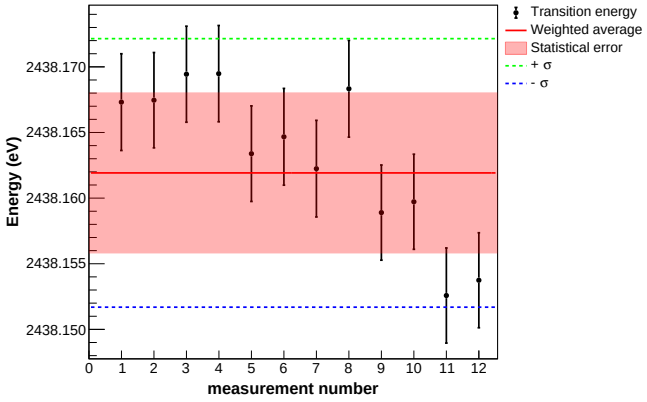


(b) $1s\ 2s\ 2p\ ^2P_{3/2} \rightarrow 1s^2\ 2s\ ^2S_{1/2}$.

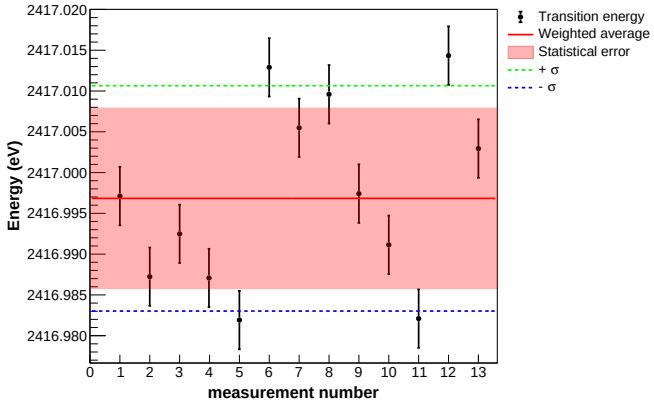


(c) $1s\ 2s\ 2p\ ^4P_{5/2} \rightarrow 1s^2\ 2s\ ^2S_{1/2}$.

FIG. 10: (Color online) Li-like sulfur $1s\ 2s\ 2p\ ^2P_J \rightarrow 1s^2\ 2s\ ^2S_{1/2}$, $J = 1/2,\ 3/2$ doublet and $1s\ 2s\ 2p\ ^4P_{5/2} \rightarrow 1s^2\ 2s\ ^2S_{1/2}$ M2 transition energy values from the different pairs of dispersive and non-dispersive spectra recorded during the experiment. Error bars correspond to statistical uncertainty obtained from Eq. (3), quadratically combined with the uncertainties in the temperature and angle measurements. The solid red curve corresponds to the weighted average, obtained considering only the statistical uncertainty in each point. The pink shaded area corresponds to the statistical uncertainty and the dashed blue and green lines ($\pm\sigma$) represent the total uncertainty obtained by the quadratically combination of the statistical uncertainty and all the instrumental contributions. Every pair of points correspond to one day of data taking.

compared with theoretical calculations. The comparison is also plotted in Fig. 14. To our knowledge this is the first measurement of these transition widths in the literature.

The comparison shows that for both elements, the $1s\ 2s\ 2p\ ^2P_{1/2} \rightarrow 1s^2\ 2s\ ^2S_{1/2}$ width is larger than that of the $1s\ 2s\ 2p\ ^2P_{3/2} \rightarrow 1s^2\ 2s\ ^2S_{1/2}$, by 97% in sulfur and 39% in argon. In contrast, all theoretical predictions give identical widths for these lines. The agreement between the experimental width of the $1s\ 2s\ 2p\ ^2P_{3/2} \rightarrow 1s^2\ 2s\ ^2S_{1/2}$ transition and theory is good. The width of the $1s\ 2s\ 2p\ ^2P_{1/2} \rightarrow 1s^2\ 2s\ ^2S_{1/2}$ transition, the less intense one, is larger than theory for both elements, an effect most exaggerated for sulfur. The width of the q and r lines has also been measured in iron in Ref. [50]. In that case the two lines were found to have nearly identical widths, in good agreement with theory. A possibility is of course a strong contamination of one of the lines from a satellite transition, that would make it appear broader. A similar problem exists for the intensity ratios. We postpone the discussion about possible contamination to Sec. IV C.

### B. Values of the energies

In Figs. 10 and 11 we present the daily energy values measured for the three transitions studied in this work, for sulfur and argon respectively. These measurements are averaged, using each pair of dispersive and

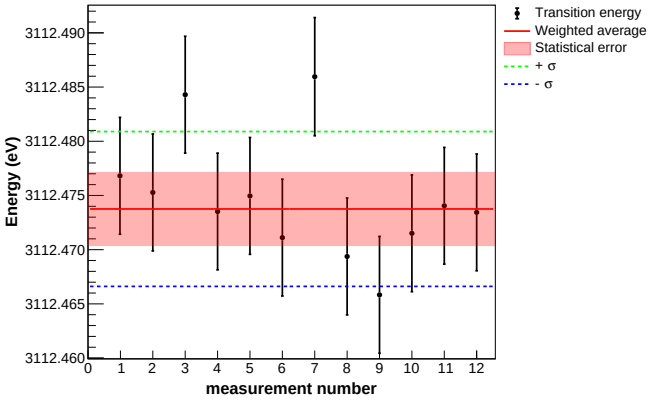


(a) $1s\ 2s\ 2p\ ^2P_{1/2} \rightarrow 1s^2\ 2s\ ^2S_{1/2}$.

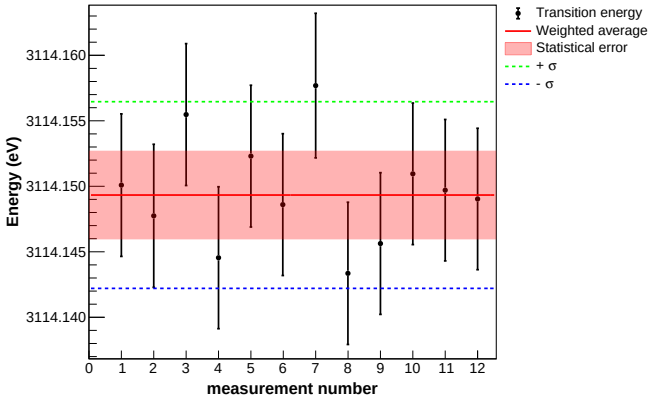


(b) $1s\ 2s\ 2p\ ^2P_{3/2} \rightarrow 1s^2\ 2s\ ^2S_{1/2}$.

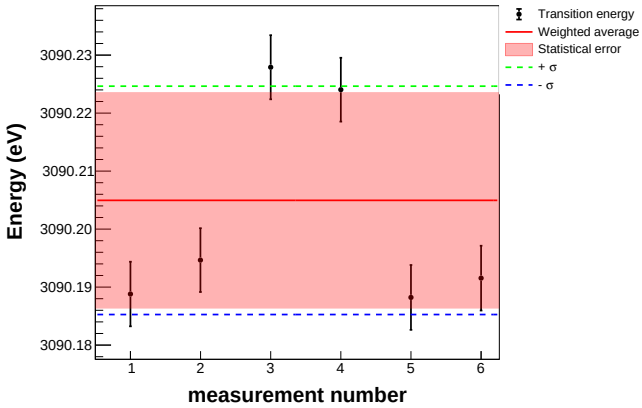


(c) $1s\ 2s\ 2p\ ^4P_{5/2} \rightarrow 1s^2\ 2s\ ^2S_{1/2}$.

FIG. 11: (Color online) Li-like argon $1s\ 2s\ 2p\ ^2P_J \rightarrow 1s^2\ 2s\ ^2S_{1/2}$, $J = 1/2,\ 3/2$ doublet and $1s\ 2s\ 2p\ ^4P_{5/2} \rightarrow 1s^2\ 2s\ ^2S_{1/2}$ M2 transition energy values for the different pairs of dispersive and non-dispersive spectra recorded during the experiment. See legend of Fig. 10 for details.

non-dispersive spectra error bars as weights. These averaged values provide the reference-free measurements of the energies of the $1s\ 2s\ 2p\ ^2P_J \rightarrow 1s^2\ 2s\ ^2S_{1/2}$ and $1s\ 2s\ 2p\ ^4P_{5/2} \rightarrow 1s^2\ 2s\ ^2S_{1/2}$ transitions. The energy of the small peak observed between the $1s\ 2s\ 2p\ ^4P_{5/2} \rightarrow 1s^2\ 2s\ ^2S_{1/2}$ and the Be-like diagram line is obtained by using the measured $1s\ 2s\ 2p\ ^4P_{5/2} \rightarrow 1s^2\ 2s\ ^2S_{1/2}$ transition energy as a reference and applying the Bragg law, as the change in shape of the spectrometer response function is negligible for such a small energy difference. We obtain an energy of 2417.345(19) eV. We compared to all the core-excited $n = 2 \rightarrow n = 1$ transitions we have evaluated with FAC for Li-like, Be-like and B-like sulfur. We find that only one transition has a significant fluorescence yield (0.97) and an energy very close to our value. It is the $1s\ 2p^2\ ^4P_{1/2} \rightarrow 1s^2\ 2p\ ^2P_{1/2}$ E1 transition in lithiumlike sulfur. The theoretical transition energy that we obtained with FAC is 2417.261 eV, and the energy provided in Ref. [32] is 2417.251(14) eV. All Be-like and B-like ions transitions with nearby energies have zero fluorescence yield. There is another Li-like line, corresponding to the $1s\ 2p^2\ ^4P_{5/2} \rightarrow 1s^2\ 2p\ ^2P_{3/2}$, with an energy of 2417.138(14) eV in Ref. [32], and 2417.132 eV in our FAC calculation, but its fluorescence yield is only 0.17. The same study in Ar did not provide evidence for this line, as the statistics of the spectra is lower.

We provide the experimental energies for the seven transitions studied in this work in Table VII. A detailed comparison with the theoretical values obtained in Sec. III and in other theoretical and experimental works is presented in Table VIII for sulfur and IX for argon. There is a generally good agreement between successives experiments and between experiment and the most advanced theoretical calculations from the present work and from Refs. [31, 32]. However some older publications, like *e.g.*, [111, 113–115] provide values that differ by ≈1 eV, because of the lack of proper QED corrections. The more recent work in Ref. [116] gives values that are very far away.

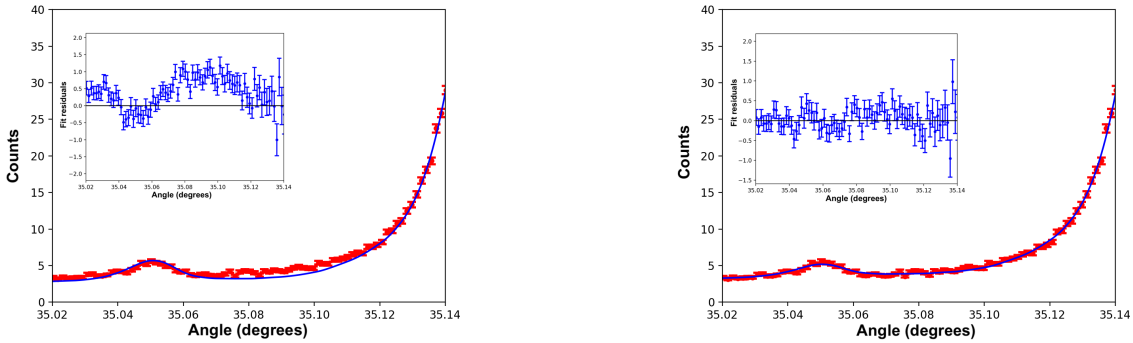


(a) no third peak

(b) with third peak

FIG. 12: (Color online) Zoom on fits to the $1s\ 2s\ 2p\ ^4P_{5/2} \rightarrow 1s^2\ 2s\ ^2S_{1/2}$ and $1s\ 2s^2\ 2p\ ^1P_1 \rightarrow 1s^2\ 2s^2\ ^1S_0$ transitions in Li-like and Be-like sulfur without (a) and with (b) inclusion of a third peak. Fitting residuals are shown for each case in the insets. See text for details.

The comparison between the very accurate measurement in Ref. [51], which are measurements relative to the heliumlike $1s\ 2s\ ^3S_1 \rightarrow 1s^2\ ^1S_0$ M1 transition, shows a shift of ≈0.053 eV in sulfur and ≈0.025 eV in argon, much larger than the combined uncertainties. The reasons for this discrepancy are currently not understood and more investigations are need to clarify the issue.

A comparison between theoretical calculations from Refs. [31, 32] and from this work, with the present experimental values shows a reasonable agreement. For argon, the agreement with Ref. [31] is compatible with the combined error bars. For sulfur, there is a larger shift. With the MCDF calculations from this work, the shifts are several times larger than the experimental uncertainty. The size of these discrepancies is compatible with the expected size of missing theoretical contributions. We can cite higher-order correlation, missing QED corrections to the electron-electron interaction (crossed-photon diagrams contributions) or approximate corrections (self-energy screening), and the Auger shift. For example, considering the $1s\ 2s\ 2p\ ^2P_{3/2} \rightarrow 1s^2\ 2s\ ^2S_{1/2}$ transition, one finds that the self-energy screening evaluated by the Welton method is 0.067 eV for sulfur and 0.091 eV for argon. If one looks at the same correction evaluated by the effective operator method, one finds 0.070 eV and 0.095 eV respectively, *i.e.*, a very small change of 0.003 eV and 0.004 eV. But if one uses the self-energy correction to the electron-electron interaction directly evaluated by QED from Ref. [119], one gets 0.091 eV and 0.122 eV. This corresponds to an increase of the transition energy by 0.024 eV in sulfur and 0.031 eV in argon, *i.e.*, 31% and 48% of the difference between experiment and theory shown in Tables VIII and IX respectively.

### C. Values for the intensity ratios of the $1s\ 2s\ 2p\ ^2P_J$ doublet

In addition to the measurement of the natural width and energy of each transition in the $1s\ 2s\ 2p\ ^2P_J$ lines

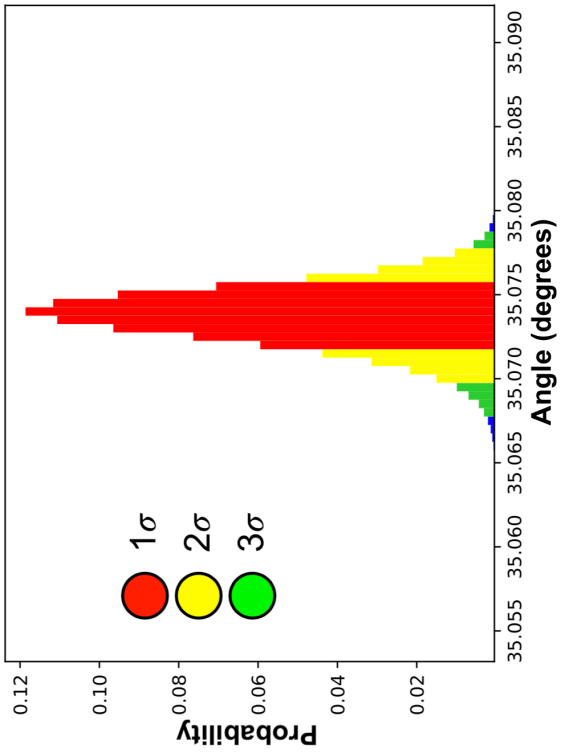


FIG. 13: (Color online) Probability of third peak position in the $1s\ 2s\ 2p\ ^4P_{5/2} \rightarrow 1s^2\ 2s\ ^2S_{1/2}$ and $1s\ 2s^2\ 2p\ ^1P_1 \rightarrow 1s^2\ 2s^2\ ^1S_0$ Li-like and Be-like sulfur doublet.

in sulfur and argon, we have been able to obtain the ratio between the intensities of the two components of this doublet. This was possible because both peaks have been measured in the same spectrum. This intensity ratio provides an experimental measurement of the relative fluorescence yields of the two transitions.

We have performed two high statistics simulations (one for each line), with the natural widths and energies of the two transitions obtained in this analysis, to fit the spectra with the function from Eq. (1). From the fit to the experimental dispersive spectrum, the optimized adjustable coefficients of the fit function were obtained from a $\chi^2$ minimization. With the coefficients provided in this procedure, the integral of each individual peak $I_1$ and $I_2$ has been numerically obtained from the equation

$$\begin{aligned} I_1 &= \int_{\theta_i}^{\theta_f} I^1_{\max} S^1_{E_{\rm Exp.},\Gamma_L^{\rm Exp.},\Gamma_G^{\rm Exp.},T_{Exp.}}(\theta-\theta_0^1)d\theta \\ I_2 &= \int_{\theta_i}^{\theta_f} I^2_{\max} S^2_{E_{\rm Exp.},\Gamma_L^{\rm Exp.},\Gamma_G^{\rm Exp.},T_{Exp.}}(\theta-\theta_0^2)d\theta, \end{aligned} \tag{7}$$

where $\theta_i$ and $\theta_f$ are the angular range of the experimental dispersive spectrum and $S^1$ and $S^2$ the interpolated simulated dispersive spectra of each transition performed with the experimental energy ($E_{\rm Exp.}$) and natural width ($\Gamma_L^{\rm Exp.}$) and the gaussian width from Ref. [18]. As a check, the numerical integration of the total fit function from Eq. (1) to the spectrum, with its background removed, has been also performed and its result compared with the sum of the individual integrals of Eq. (7). The numerical integrals have been calculated with the data analysis framework ROOT from CERN [120–122] through the MathMore library. This library uses the integration algorithms of GSL [123], which reimplements the algorithms used in the QUADPACK [124], a numerical integration package written in Fortran. In Figs. 15 and 16 an example of the numerical integration to a dispersive spectra of the Li-like doublet transition in argon is presented. The total integral fit is represented by the solid black curve and the corresponding integral is represented by the shadowed white area with the wave-like texture. The individual peak fits are represented by the red ($J = 1/2$) and green ($J = 3/2$) solid curves, and their respective integrals are shown as the shadowed areas with the same

TABLE II: Theoretical contributions to the sulfur transition energies, as evaluated with the MCDFGME code. All energies are given in eV.

| Contribution | $1s\ 2s\ 2p\ ^2P_{1/2} \rightarrow 1s^2 2s\ ^2S_{1/2}$ | $1s\ 2s\ 2p\ ^2P_{3/2} \rightarrow 1s^2 2s\ ^2S_{1/2}$ | $1s\ 2s\ 2p\ ^4P_{5/2} \rightarrow 1s^2 2s\ ^2S_{1/2}$ |
|---|---|---|---|
| Coulomb+ Uelhing | 2438.584 | 2439.638 | 2418.121 |
| Magnetic | −1.423 | −1.444 | −1.435 |
| Retardation | 0.049 | 0.053 | −0.049 |
| Higher-order retardation | 0.001 | 0.001 | −0.001 |
| Self-energy | −0.811 | −0.808 | −0.806 |
| Self-energy screening | 0.068 | 0.070 | 0.077 |
| Uelhing (muon pairs) | 0.000 | 0.000 | 0.000 |
| Electronic density Uelhing | −0.001 | −0.001 | −0.001 |
| Wichmann and Kroll | 0.000 | 0.000 | 0.000 |
| Källèn and Sabry | 0.000 | 0.000 | 0.000 |
| Two-loop self-energy | 0.000 | 0.000 | 0.000 |
| SEVP | 0.000 | 0.000 | 0.000 |
| S(VP)E | 0.000 | 0.000 | 0.000 |
| Normal mass shift | 0.000 | 0.000 | 0.000 |
| Specific mass shift | −0.042 | −0.042 | −0.041 |
| Relativistic recoil | 0.005 | 0.007 | −0.008 |
| Coulomb correlation | 0.584 | 0.542 | 1.011 |
| Magnetic correlation | 0.105 | 0.104 | 0.127 |
| retardation correlation | −0.028 | −0.029 | −0.030 |
| Higher-order ret. Corr. | 0.000 | 0.000 | 0.000 |
| Total | 2437.091 | 2438.091 | 2416.964 |

TABLE III: Theoretical contributions to the argon transition energies, as evaluated with the MCDFGME code. All energies are given in eV.

| Contribution | $1s\ 2s\ 2p\ ^2P_{1/2} \rightarrow 1s^2 2s\ ^2S_{1/2}$ | $1s\ 2s\ 2p\ ^2P_{3/2} \rightarrow 1s^2 2s\ ^2S_{1/2}$ | $1s\ 2s\ 2p\ ^4P_{5/2} \rightarrow 1s^2 2s\ ^2S_{1/2}$ |
|---|---|---|---|
| Coulomb+ Uelhing | 3114.855 | 3116.647 | 3092.248 |
| Magnetic | −2.023 | −2.088 | −2.062 |
| Retardation | 0.069 | 0.078 | −0.071 |
| Higher-order retardation | 0.001 | 0.001 | −0.002 |
| Self-energy | −1.218 | −1.213 | −1.211 |
| Self-energy screening | 0.090 | 0.095 | 0.104 |
| Uelhing (muon pairs) | 0.000 | 0.000 | 0.000 |
| Electronic density Uelhing | −0.001 | −0.001 | −0.001 |
| Wichmann and Kroll | 0.000 | 0.000 | 0.000 |
| Källèn and Sabry | 0.001 | 0.001 | 0.001 |
| Two-loop self-energy | 0.000 | 0.000 | 0.000 |
| SEVP | 0.000 | 0.000 | 0.000 |
| S(VP)E | 0.000 | 0.000 | 0.000 |
| Normal mass shift | 0.000 | 0.000 | 0.000 |
| Specific mass shift | −0.042 | −0.042 | −0.042 |
| Relativistic recoil | 0.005 | 0.007 | −0.008 |
| Coulomb correlation | 0.579 | 0.526 | 0.984 |
| Magnetic correlation | 0.128 | 0.130 | 0.152 |
| Retardation correlation | −0.033 | −0.036 | −0.035 |
| Higher-order ret. Corr. | 0.000 | 0.000 | 0.000 |
| Total | 3112.411 | 3114.104 | 3090.056 |

color. The background has been removed from the integrals and the obtained values for the integrals are presented in the legend with the respective estimated error. The estimated error in the integration is due to the uncertainties of each adjustable coefficient of the fit function optimized by the $\chi^2$ minimization.

The integration of each peak area has been performed for all dispersive spectra. The ratio between the intensities of the $1s\ 2s\ 2p\ ^2P_{1/2} \rightarrow 1s^2\ 2s\ ^2S_{1/2}$ and $1s\ 2s\ 2p\ ^2P_{3/2} \rightarrow 1s^2\ 2s\ ^2S_{1/2}$ transitions are presented in Figs. 17 and 18 for all recorded dispersive spectra of sulfur and argon, respectively. The weighted average is represented by the solid red line and the $\pm\sigma$ values are represented by the green and blue dashed lines. The

TABLE IV: Theoretical sulfur radiative and Auger lifetimes, energies and fluorescence yields, as evaluated with the MCDFGME code. All E$n$ and M$n$ multipole contributions are included for the radiative transitions. All widths are given in meV and energies in eV.

| Final level | $1s\ 2s\ 2p\ ^2P_{1/2}$ | | $1s\ 2s\ 2p\ ^2P_{3/2}$ | | $1s\ 2s\ 2p\ ^4P_{5/2}$ | | Type |
|---|---|---|---|---|---|---|---|
| | Width | Energy | Width | Energy | Width | Energy | |
| $1s^2\ 2s\ ^2S_{1/2}$ | 35.08457 | 2437.090 | 38.93449 | 2438.090 | $7.132 \times 10^{-5}$ | 2416.963 | Radiative |
| All $1s^2\ 2pj$ | 0.00001 | | 0.00001 | | $8.390 \times 10^{-7}$ | | Radiative |
| All $1s^2\ 3lj$ | 0.01086 | | 0.01305 | | $2.609 \times 10^{-8}$ | | Radiative |
| All $1s^2\ 4lj$ | 0.00152 | | 0.00189 | | $3.897 \times 10^{-9}$ | | Radiative |
| All $1s^2\ 5lj$ | 0.00049 | | 0.00062 | | $1.289 \times 10^{-9}$ | | Radiative |
| All $1s^2\ 6lj$ | 0.00023 | | 0.00029 | | $5.929 \times 10^{-10}$ | | Radiative |
| All $1s^2\ 7lj$ | 0.00021 | | 0.00016 | | $3.258 \times 10^{-10}$ | | Radiative |
| Total | 0.01330 | | 0.01602 | | $8.712 \times 10^{-7}$ | | Radiative |
| $1s^2\ ^1S_0$ | 3.1432 | 1730.106 | 0.00006 | 1731.106 | $5.579 \times 10^{-4}$ | 1709.972 | Auger |
| Total width | 38.24107 | | 38.95057 | | $6.300 \times 10^{-4}$ | | |
| Fluorescence yield | 0.917 | | 1.000 | | 0.113 | | |

TABLE V: Theoretical argon radiative and Auger lifetimes, energies and fluorescence yields, as evaluated with the MCDFGME code. All E$n$ and M$n$ multipole contributions are included for the radiative transitions. All widths are given in meV and energies in eV.

| Final level | $1s\ 2s\ 2p\ ^2P_{1/2}$ | | $1s\ 2s\ 2p\ ^2P_{3/2}$ | | $1s\ 2s\ 2p\ ^4P_{5/2}$ | | Type |
|---|---|---|---|---|---|---|---|
| | Width | Energy | Width | Energy | Width | Energy | |
| $1s^2\ 2s\ ^2S_{1/2}$ | 55.98473 | 3112.410 | 65.0552 | 3111.194 | $1.916 \times 10^{-4}$ | 3114.100 | Radiative |
| All $1s^2\ 2pj$ | 0.00001 | | 0.00002 | | $2.855 \times 10^{-6}$ | | Radiative |
| All $1s^2\ 3lj$ | 0.01310 | | 0.01703 | | $5.482 \times 10^{-8}$ | | Radiative |
| All $1s^2\ 4lj$ | 0.00179 | | 0.00246 | | $8.101 \times 10^{-9}$ | | Radiative |
| All $1s^2\ 5lj$ | 0.00058 | | 0.00081 | | $2.667 \times 10^{-9}$ | | Radiative |
| All $1s^2\ 6lj$ | 0.00026 | | 0.00038 | | $1.224 \times 10^{-9}$ | | Radiative |
| All $1s^2\ 7lj$ | 0.00014 | | 0.00021 | | $6.716 \times 10^{-10}$ | | Radiative |
| Total | 0.01588 | | 0.02091 | | $2.922 \times 10^{-6}$ | | Radiative |
| $1s^2\ ^1S_0$ | 7.1881 | 2194.053 | 0.0094 | 2195.743 | $9.229 \times 10^{-4}$ | 2171.716 | Auger |
| Total width | 63.18875 | | 65.08545 | | $1.117 \times 10^{-3}$ | | |
| Fluorescence yield | 0.886 | | 1.000 | | 0.171 | | |

ratio between the two transitions is 0.603(21) for sulfur and 0.358(13) for argon. Yet, as discussed in [125], the number of x rays from a given transition that reach the detector in a DCS does not depend only on the balance between the feeding mechanisms and the radiative transition intensity, but also on the geometrical settings, on the shape of the collimator and on the angular acceptance of the first Bragg crystal. The transmission functions for the energy range 2430 eV to 2445 eV in sulfur and 3085 eV to 3125 eV in argon are presented in Fig. 19. Because the dispersion is much higher for sulfur and the absorption in the crystal is higher, the curve for sulfur is asymmetric. The curve for sulfur was thus fitted with splines to obtain a transmission value for the $1s\ 2s\ 2p\ ^2P_{1/2} \rightarrow 1s^2\ 2s\ ^2S_{1/2}$ and $1s\ 2s\ 2p\ ^2P_{3/2} \rightarrow 1s^2\ 2s\ ^2S_{1/2}$ lines. One gets the spectrometer correction to the line intensities

$$\frac{I_{E_{J=1/2}}}{I_{E_{J=3/2}}} = 1.0399, \tag{8}$$

by inserting the experimental values of the line energies from Table VIII into the spline fit. Applying this correction to the value shown in Fig. 17 we obtain a ratio of 0.627(22) for the relative intensities of the two lines in Li-like sulfur.

For argon, we were able to fit the symmetric curve and found the normalized hyperbolic expression [125]

$$\begin{aligned} I(E) =& 1.04815 - 6.27647 \times 10^{-5} \\ & \times \sqrt{|588509 + 690026(E - 3103.89)^2|}. \end{aligned} \tag{9}$$

Entering the line energies in Eq. 9 we obtain the correction

$$\frac{I_{E_{J=1/2}}}{I_{E_{J=3/2}}} = 1.1091, \tag{10}$$

which, multiplied by the ratio between the peak intensities given in Fig. 18, gives the final value of 0.397(14).

Assuming a statistical population of the levels, the fluorescence yield of Tables IV and V leads to an intensity ratio of 0.46 for sulfur and 0.44 for argon. This is consis-

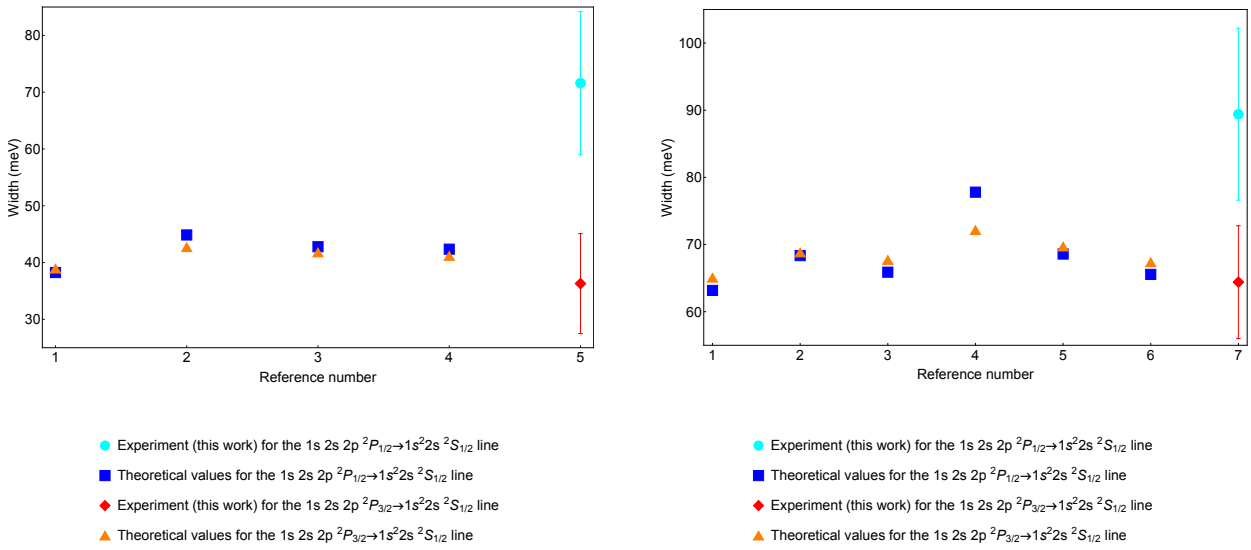


(a) Sulfur doublet widths

(b) Argon doublet widths

FIG. 14: (Color online) Comparison between the measured and theoretical values for the widths. Sulfur references: 1, This work, MCDF; 2, this work FAC; 3, Ref. [110]; 4, Ref. [111]; 5, this work, experiment. Argon references: 1, This work, MCDF; 2, this work FAC; 3, Ref. [110]; 4, Ref. [112]; 5, Ref. [113]; 6, Ref. [111]; 7, this work, experiment.

TABLE VI: Comparison between experimental and theoretical Li-like sulfur and argon $1s\ 2s\ 2p\ ^2P_J$, $J = 1/2,\ 3/2$ and $1s\ 2s\ 2p\ ^4P_{5/2}$ level widths. All values are given in meV.

| Element | Level | Exp. width | Err. | Th. width | Ref. |
|---|---|---|---|---|---|
| S | $1s\ 2s\ 2p\ ^2P_{1/2} \rightarrow 1s^2\ 2s\ ^2S_{1/2}$ | 71.6 | 12.6 | 38.2 | This work (MCDF) |
| | | | | 44.9 | This work (FAC) |
| | | | | 42.8 | [110] |
| | | | | 42.4 | [111] |
| S | $1s\ 2s\ 2p\ ^2P_{3/2} \rightarrow 1s^2\ 2s\ ^2S_{1/2}$ | 36.3 | 8.8 | 38.9 | This work (MCDF) |
| | | | | 42.7 | This work (FAC) |
| | | | | 41.8 | [110] |
| | | | | 41.2 | [111] |
| Ar | $1s\ 2s\ 2p\ ^2P_{1/2} \rightarrow 1s^2\ 2s\ ^2S_{1/2}$ | 89.4 | 12.8 | 63.2 | This work (MCDF) |
| | | | | 68.4 | This work (FAC) |
| | | | | 65.9 | [110] |
| | | | | 77.8 | [112] |
| | | | | 68.6 | [113] |
| | | | | 65.6 | [111] |
| Ar | $1s\ 2s\ 2p\ ^2P_{3/2} \rightarrow 1s^2\ 2s\ ^2S_{1/2}$ | 64.4 | 8.4 | 65.1 | This work (MCDF) |
| | | | | 68.8 | This work (FAC) |
| | | | | 67.7 | [110] |
| | | | | 72.2 | [112] |
| | | | | 69.7 | [113] |
| | | | | 67.4 | [111] |

tent with the experimental value for argon, but not for sulfur.

To understand this difference, we have investigated possible line blends, as presented in Figs. 20 for sulfur and 21 for argon. We considered at the same time other Li-like lines, as well as Be-like and B-like ones. For Li-like lines we used transition energies from Refs. [31, 32]. The relative intensities have been obtained using FAC and evaluating all possible radiative and Auger transitions for a given initial level. For argon, these calculations are in good agreement with the results from Ref. [112].

For sulfur (Fig. 20) the $1s\ 2p^2\ ^2P_{3/2} \rightarrow 1s^2\ 2p\ ^2P_{1/2}$

TABLE VII: Experimental values of the energies for the seven lines measured in this work. All energies are given in eV. All energies presented here are reference-free values, except for the $1s\ 2p^2\ ^4P_{1/2} \rightarrow 1s^2\ 2p\ ^2P_{1/2}$ transition in sulfur, which is measured relative to the $1s\ 2s\ 2p\ ^4P_{5/2} \rightarrow 1s^2\ 2s\ ^2S_{1/2}$ transition.

| Element | transition | Energy | Stat. uncer. | Syst. uncer. | Tot. uncer. | ppm |
|---|---|---|---|---|---|---|
| S | $1s\ 2s\ 2p\ ^2P_{1/2} \rightarrow 1s^2\ 2s\ ^2S_{1/2}$ | 2437.1658 | 0.0068 | 0.0082 | 0.011 | 4.4 |
| S | $1s\ 2s\ 2p\ ^2P_{3/2} \rightarrow 1s^2\ 2s\ ^2S_{1/2}$ | 2438.1619 | 0.0061 | 0.0082 | 0.010 | 4.2 |
| S | $1s\ 2s\ 2p\ ^4P_{5/2} \rightarrow 1s^2\ 2s\ ^2S_{1/2}$ | 2416.997 | 0.011 | 0.0082 | 0.014 | 5.7 |
| S | $1s\ 2p^2\ ^4P_{1/2} \rightarrow 1s^2\ 2p\ ^2P_{1/2}$ | 2417.345 | 0.017 | 0.0082 | 0.019 | 7.8 |
| Ar | $1s\ 2s\ 2p\ ^2P_{1/2} \rightarrow 1s^2\ 2s\ ^2S_{1/2}$ | 3112.4737 | 0.0034 | 0.0063 | 0.0071 | 2.3 |
| Ar | $1s\ 2s\ 2p\ ^2P_{3/2} \rightarrow 1s^2\ 2s\ ^2S_{1/2}$ | 3114.1493 | 0.0034 | 0.0063 | 0.0071 | 2.3 |
| Ar | $1s\ 2s\ 2p\ ^2P_{5/2} \rightarrow 1s^2\ 2s\ ^2S_{1/2}$ | 3090.205 | 0.019 | 0.0063 | 0.020 | 6.4 |

TABLE VIII: Comparison between the reference-free measurements from this work and theoretical and experimental transition energies for lithiumlike sulfur. TW: this work. All energies are given in eV. Diff.: energy difference between this work's experimental value and theory.

| Experiment | | | | Theory | | | |
|---|---|---|---|---|---|---|---|
| Transition | Energy | Unc. | Ref. | Energy | Unc. | Diff. | Ref. |
| $1s\ 2s\ 2p\ ^2P_{1/2}$ | 2437.166 | 0.011 | TW | 2437.087 | | 0.079 | TW (Welton) |
| $\rightarrow 1s^2\ 2s\ ^2S_{1/2}$ | 2437.115 | 0.005 | [51] | 2437.090 | | 0.076 | TW (Eff. Op.) |
| | 2437.71 | 0.24 | [37] | 2437.056 | | 0.110 | TW FAC |
| | | | | 2437.1 | | 0.066 | [110] |
| | | | | 2437.074 | 0.019 | 0.092 | [32] |
| | | | | 2437.51 | | −0.349 | [111] |
| | | | | 2437.20 | | −0.037 | [117] |
| $1s\ 2s\ 2p\ ^2P_{3/2}$ | 2438.162 | 0.010 | TW | 2438.087 | | 0.075 | TW (Welton) |
| $\rightarrow 1s^2\ 2s\ ^2S_{1/2}$ | 2438.106 | 0.003 | [37] | 2438.090 | | 0.072 | TW (Eff. Op.) |
| | | | | 2438.065 | | 0.097 | TW FAC |
| | | | | 2438.066 | 0.019 | 0.096 | [32] |
| | | | | 2438.0 | | 0.162 | [110] |
| | | | | 2438.17 | | −0.005 | [117] |
| | | | | 2438.47 | | −0.312 | [111] |
| $1s\ 2s\ 2p\ ^4P_{5/2}$ | 2416.997 | 0.014 | TW | 2416.959 | | 0.038 | TW (Welton) |
| $\rightarrow 1s^2\ 2s\ ^2S_{1/2}$ | | | | 2416.963 | | 0.034 | TW (Eff. Op.) |
| | | | | 2416.286 | | 0.711 | TW FAC |
| | | | | 2417.162 | | −0.166 | [117] |
| | | | | 2416.963 | 0.019 | 0.034 | [32] |

transition is blended with the lower energy member of the observed doublet, the $1s\ 2s\ 2p\ ^2P_{1/2} \rightarrow 1s^2\ 2s\ ^2S_{1/2}$ transition, with a difference of energy of only 0.07 eV. However this line has a relative intensity of only 7.53%. The other intense line originating from the same level as the $1s\ 2p^2\ ^2P_{3/2} \rightarrow 1s^2\ 2p\ ^2P_{3/2}$ line has a relative intensity of 85.4%, but it lies outside the window of energy scanned during the experiment. Yet this line is not observed in argon, while it is in the scanned area (see Fig. 21). It is thus highly unlikely, with two elements so close in $Z$, that the contamination would be more significant in sulfur than in argon. Figure 20 shows that no Be-like and B-like core-excited transitions have a relative intensity able to explain the difference between S and Ar.

In argon, as seen in Fig. 21, the higher energy component of the doublet, the $1s\ 2s\ 2p\ ^2P_{3/2} \rightarrow 1s^2\ 2s\ ^2S_{1/2}$ is blended with the $1s\ 2p^2\ ^2P_{3/2} \rightarrow 1s^2\ 2p\ ^2P_{1/2}$ transition (the energy difference is 0.26 eV). Yet it has a relative intensity of only 5.4%, while the other intense line originating from the same level, the $1s\ 2p^2\ ^2P_{3/2} \rightarrow 1s^2\ 2p\ ^2P_{3/2}$ one, has a relative intensity of 87%. Since no line is seen at the expected position, we conclude that this blend cannot explain the difference. The figure also shows that, as observed in sulfur, no Be-like or B-like line can change the relative intensity of the $1s\ 2s\ 2p\ ^2P_J \rightarrow 1s^2\ 2s\ ^2S_{1/2}$ doublet.

Both sulfur and argon lithiumlike doublets were also tested for the presence of a third contaminant peak, using the method described in Subsec. II B 3. Bayesian evidence was evaluated for two models : i) the two simulated response functions superimposed on a linear background, as used in the aforementioned analysis ii) the two simulated response functions are superimposed on a linear background and a third Voigt peak. The Doppler broadening of the Voigt peak was fixed to 90 meV, consistent with the broadening of the S He-like M1 peak,

TABLE IX: Comparison between the reference-free measurements from this work and theoretical and experimental transition energies for lithiumlike argon. TW: this work. All energies are given in eV. Diff.: energy difference between this work's experimental value and theory.

| Experiment | | | | Theory | | | |
|---|---|---|---|---|---|---|---|
| Transition | Energy | Unc. | Ref. | Energy | Unc. | Diff. | Ref. |
| $1s\ 2s\ 2p\ ^2P_{1/2}$ | 3112.4737 | 0.0071 | TW | 3112.409 | | 0.065 | TW (Welton) |
| $\rightarrow 1s^2\ 2s\ ^2S_{1/2}$ | 3112.4510 | 0.0020 | [51] | 3112.410 | | 0.064 | TW Eff. Op. |
| | 3112.63 | 0.16 | [37] | 3112.360 | | 0.113 | TW FAC |
| | 3112.4203 | 0.0859 | [47] | 3112.40 | | 0.074 | [110] |
| | 3112.405 | 0.078 | [46] | 3112.471 | 0.012 | 0.003 | [31] |
| | 3111.795 | 0.305 | [49] | 3113.07 | | −0.595 | [111] |
| | | | | 3112.29 | | 0.184 | [118] |
| | | | | 3114.70 | | −2.226 | [114] |
| | | | | 3111.19 | | 1.280 | [115] |
| | | | | 3110.74 | | 1.732 | [113] |
| | | | | 3112.60 | | −0.127 | [117] |
| | | | | 3118.04 | | −5.562 | [116] |
| | | | | 3112.40 | | 0.074 | [112] |
| $1s\ 2s\ 2p\ ^2P_{3/2}$ | 3114.1493 | 0.0071 | TW | 3114.098 | | 0.051 | TW (Welton) |
| $\rightarrow 1s^2\ 2s\ ^2S_{1/2}$ | 3114.1220 | 0.0020 | [51] | 3114.103 | | 0.046 | TW Eff. Op. |
| | 3114.190 | 0.078 | [37] | 3114.061 | | 0.088 | TW FAC |
| | 3114.132 | 0.078 | [46] | 3114.1417 | 0.0055 | 0.008 | [31] |
| | 3114.078 | 0.086 | [47] | 3114.10 | | 0.049 | [110] |
| | 3113.97 | 0.12 | [49] | 3114.22 | | −0.075 | [117] |
| | | | | 3114.71 | | −0.562 | [111] |
| | | | | 3114.01 | | 0.139 | [118] |
| | | | | 3116.40 | | −2.251 | [114] |
| | | | | 3113.07 | | 1.080 | [115] |
| | | | | 3112.44 | | 1.713 | [113] |
| | | | | 3119.69 | | −5.540 | [116] |
| | | | | 3114.15 | | −0.001 | [112] |
| $1s\ 2s\ 2p\ ^4P_{5/2}$ | 3090.205 | 0.020 | TW | 3090.050 | | 0.155 | TW (Welton) |
| $\rightarrow 1s^2\ 2s\ ^2S_{1/2}$ | 3090.25 | 0.12 | [47] | 3090.055 | | 0.150 | TW Eff. Op. |
| | 3091.0 | 2.0 | [54] | 3089.374 | | 0.831 | TW FAC |
| | | | | 3090.32 | | −0.114 | [117] |
| | | | | 3089.31 | | 0.895 | [118] |
| | | | | 3090.10 | | 0.105 | [114] |
| | | | | 3090.1456 | 0.0046 | 0.059 | [31] |

while the Lorentzian width was left free and the centroid allowed to be anywhere in the spectrum. The bayesian evidence was significantly higher when a third peak was added with a gain in ln(evidence) of 60.62(8) and 10.55(9) for the lithiumlike S and Ar doublets, respectively. The corresponding $p$-factors are approximately $2.63 \times 10^{-29}$ and $2.78 \times 10^{-7}$, respectively. However, in both cases the ratio of intensities between the third peak and the $1s\ 2s\ 2p\ ^2P_{1/2} \rightarrow 1s^2\ 2s\ ^2S_{1/2}$ transition was found to be less than 1 %, and the centroid of the third peak far to the left of the line, and thus unable to explain the intensity discrepancy seen in the data.

We can now come back to the difference in width between the two components of the $1s\ 2s\ 2p\ ^2P_J \rightarrow 1s^2\ 2s\ ^2S_{1/2}$ doublet discussed in IV A. The absence of contamination discussed above shows that the difference in width observed between the two lines of the doublet, cannot be explained by the presence of other unresolved lines.

## V. CONCLUSION

We have made the first reference-free measurement of the two allowed $1s\ 2s\ 2p\ ^2P_{3/2} \rightarrow 1s^2\ 2s\ ^2S_{1/2}$ and $1s\ 2s\ 2p\ ^2P_{1/2} \rightarrow 1s^2\ 2s\ ^2S_{1/2}$ transitions, and of the forbidden $1s\ 2s\ 2p\ ^4P_{5/2} \rightarrow 1s^2\ 2s\ ^2S_{1/2}$ M2 transition in core-excited lithiumlike sulfur and argon. Our results have accuracies comparable to those of the best available relative measurements [51]. Up to now the M2 transitions has been known only in argon, with a 3-times larger uncertainty. We also measured the energy of the $1s\ 2p^2\ ^4P_{1/2} \rightarrow 1s^2\ 2p\ ^2P_{1/2}$ transition in Li-like sulfur, relative to the $1s\ 2s\ 2p\ ^4P_{5/2} \rightarrow 1s^2\ 2s\ ^2S_{1/2}$ transition. We have also measured the width and the intensity ratios of the $1s\ 2s\ 2p\ ^2P_{3/2} \rightarrow 1s^2\ 2s\ ^2S_{1/2}$ and $1s\ 2s\ 2p\ ^2P_{1/2} \rightarrow 1s^2\ 2s\ ^2S_{1/2}$ line doublet. The agreement between our experimental energies and the most-comprehensive, state of the art theoretical values (this

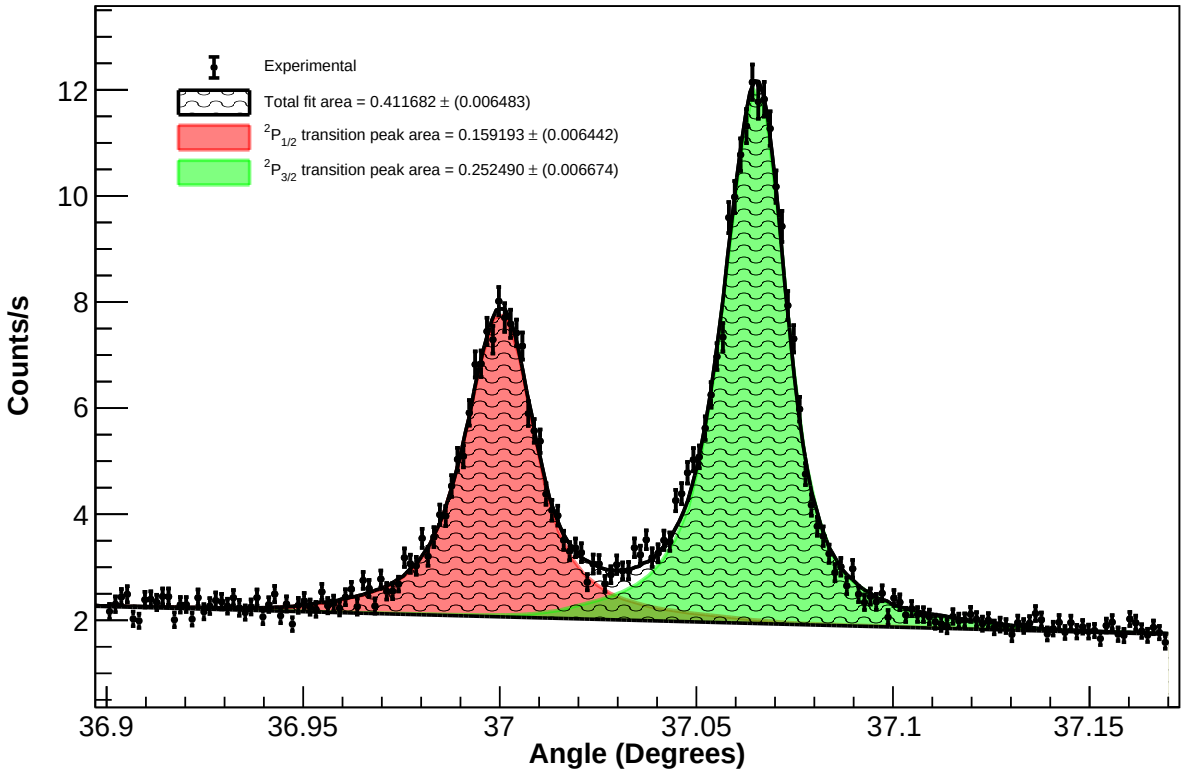


FIG. 15: (Color online) Integral example of the Li-like sulfur $1s\ 2s\ 2p\ ^2P_J \rightarrow 1s^2\ 2s\ ^2S_{1/2}$, $J = 1/2,\ 3/2$ doublet dispersive spectrum. The solid black curve represents the total fit to the spectrum from Eq. (1) with its respective integral represented by the shadowed white area with the wave-like texture. Red ($J = 1/2$) and green ($J = 3/2$) solid curves represent the individual fits to each peak while the individual integrals are represented by the shadowed areas with the same color. The values obtained for the integrals with their respective estimated error are presented in the plot legend.

work and [31]) is within the combined error bars for argon. It is not as good for sulfur (Ref. [32] and this work). The differences are probably due to the missing correlation contributions, larger at lower $Z$, to missing QED corrections and to Auger shifts. More high-accuracy measurements of these transitions for other elements are required to better understand the reasons for the discrepancy between experiment and theory.

The width of the $1s\ 2s\ 2p\ ^2P_{3/2} \rightarrow 1s^2\ 2s\ ^2S_{1/2}$ transition agrees with theory for both sulfur and argon, while the width of the $1s\ 2s\ 2p\ ^2P_{1/2} \rightarrow 1s^2\ 2s\ ^2S_{1/2}$ transition disagrees. This width discrepancy is not observed in iron [50]. We have been able to exclude contaminations by other lines as a cause for this discrepancy. Moreover the $1s\ 2s\ 2p\ ^2P_J \rightarrow 1s^2\ 2s\ ^2S_{1/2}$ transitions intensity ratios do not agree with theory. In the future we plan to measure these transitions in other elements like chlorine and $Z > 18$ to have a better idea of the evolution of the widths and intensity ratios as a function of $Z$.

## ACKNOWLEDGMENTS

This research was supported in part by the projects No. PEstOE/FIS/UI0303/2011, PTDC/FIS/117606/2010 and PTDC/FIS-AQM/31969/2017, and by the research centre grant No. UID/FIS/04559/2013 (LIBPhys), from FCT/MCTES/PIDDAC, Portugal. P.A., J.M., and M.G. acknowledge support from FCT, under Contracts No. SFRH/BPD/92329/2013, No. SFRH/BD/52332/2013, and No. SFRH-/BPD/92455/2013 respectively. Laboratoire Kastler Brossel (LKB) is a *Unité Mixte de Recherche de Sorbonne University-UPMC, de ENS-PSL Research University, du Collège de France et du CNRS n° 8552'.*

P.I. is a member of the Allianz Program of the Helmholtz Association, contract n° EMMI HA-216 "Extremes of Density and Temperature: Cosmic Matter in the Laboratory". Part of this work has been performed during stays financed by the Programme Hubert Curien PESSOA 38028UD and program PAUILF 2017-

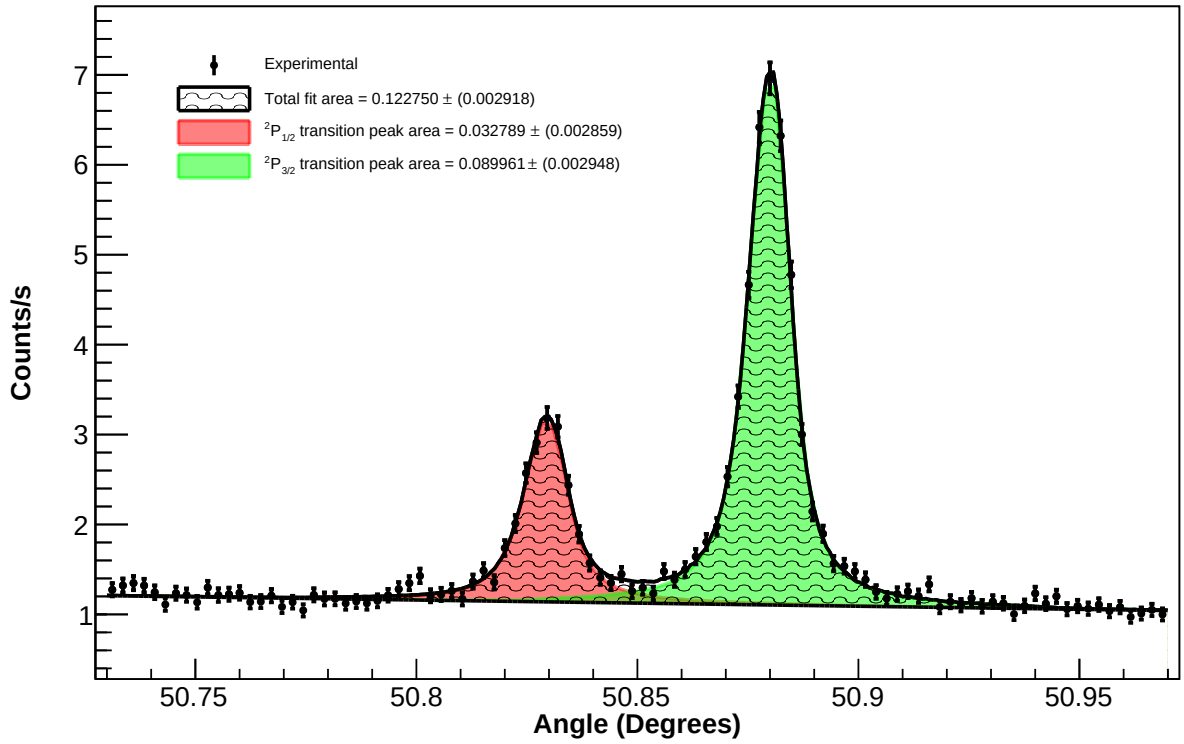


FIG. 16: (Color online) Integral example of the Li-like argon $1s\ 2s\ 2p\ ^2P_J \rightarrow 1s^2\ 2s\ ^2S_{1/2}$, $J = 1/2,\ 3/2$ doublet dispersive spectrum. The solid black curve represents the total fit to the spectrum from Eq. (1) with its respective integral represented by the shadowed white area with the wave-like texture. Red ($J = 1/2$) and green ($J = 3/2$) solid curves represent the individual fits to each peak while the individual integrals are represented by the shadowed areas with the same color. The values obtained for the integrals with the respective estimated error are presented in the plot legend.

C08. The SIMPA ECRIS has been financed by grants from CNRS, MESR, and UPMC. The experiment has been supported by grants from BNM 01 3 0002 and the ANR ANR-06-BLAN-0223. P.I. acknowledges support from the Institute of Physics of the CNRS for the post-doc positions provided during the course of this work.

[1] P. Indelicato, J. Phys. B: At. Mol. Opt. Phys. **52**, 232001 (2019), URL https://doi.org/10.1088/1361-6455/ab42c9.

[2] C. G. Parthey, A. Matveev, J. Alnis, B. Bernhardt, A. Beyer, R. Holzwarth, A. Maistrou, R. Pohl, K. Predehl, T. Udem, et al., Phys. Rev. Lett. **107**, 203001 (2011), URL http://link.aps.org/doi/10.1103/PhysRevLett.107.203001.

[3] A. Beyer, L. Maisenbacher, A. Matveev, R. Pohl, K. Khabarova, A. Grinin, T. Lamour, D. C. Yost, T. W. Hänsch, N. Kolachevsky, et al., Science **358**, 79 (2017), URL http://science.sciencemag.org/content/sci/358/6359/79.full.pdf.

[4] H. Fleurbaey, S. Galtier, S. Thomas, M. Bonnaud, L. Julien, F. Biraben, F. Nez, M. Abgrall, and J. Guéna, Phys. Rev. Lett. **120**, 183001 (2018), URL https://link.aps.org/doi/10.1103/PhysRevLett.120.183001.

[5] H. Häffner, T. Beier, N. Hermanspahn, H.-J. Kluge, W. Quint, S. Stahl, J. Verdú, and G. Werth, Phys. Rev. Lett. **85**, 5308 (2000), URL https://journals.aps.org/prl/abstract/10.1103/PhysRevLett.85.5308.

[6] S. Sturm, F. Kohler, J. Zatorski, A. Wagner, Z. Harman, G. Werth, W. Quint, C. H. Keitel, and K. Blaum, Nature **506**, 467 (2014), URL http://dx.doi.org/10.1038/nature13026.

[7] F. Köhler, S. Sturm, A. Kracke, G. Werth, W. Quint, and K. Blaum, J. Phys. B: At. Mol. Opt. Phys. **48**, 144032 (2015), URL http://stacks.iop.org/0953-4075/48/i=14/a=144032.

[8] J. Zatorski, B. Sikora, S. G. Karshenboim, S. Sturm, F. Köhler-Langes, K. Blaum, C. H. Keitel, and Z. Har-

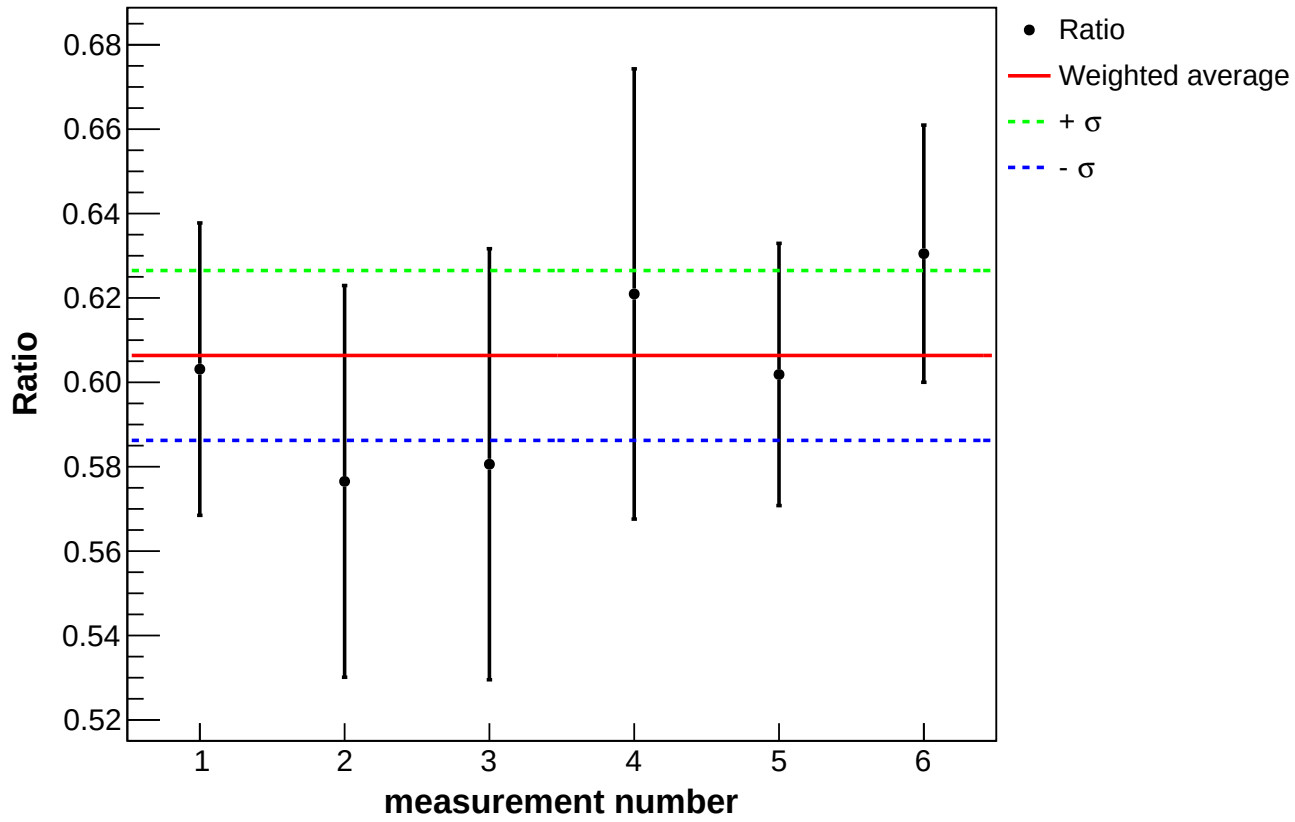


FIG. 17: (Color online) Ratio between the $1s\ 2s\ 2p\ ^2P_{1/2} \rightarrow 1s^2\ 2s\ ^2S_{1/2}$ and $1s\ 2s\ 2p\ ^2P_{3/2} \rightarrow 1s^2\ 2s\ ^2S_{1/2}$ transition intensities for all recorded dispersive spectra in sulfur. The weighted average value of 0.603 is represented by the solid red line and the $\pm\sigma = 0.021$ are represented by the green and blue dashed lines. The error bar at each point corresponds to the contribution of the uncertainty from the numerical integration of each peak.

man, Phys. Rev. A **96**, 012502 (2017), URL https://link.aps.org/doi/10.1103/PhysRevA.96.012502.

[9] J. Verdu, S. Djekic, S. Stahl, T. Valenzuela, M. Vogel, G. Werth, T. Beier, H.-J. Kluge, and W. Quint, Phys. Rev. Lett. **92**, 093002 (2004), URL http://link.aps.org/abstract/PRL/v92/e093002.

[10] S. Sturm, A. Wagner, B. Schabinger, J. Zatorski, Z. Harman, W. Quint, G. Werth, C. H. Keitel, and K. Blaum, Phys. Rev. Lett. **107**, 023002 (2011), URL http://link.aps.org/doi/10.1103/PhysRevLett.107.023002.

[11] S. Sturm, A. Wagner, M. Kretzschmar, W. Quint, G. Werth, and K. Blaum, Phys. Rev. A **87**, 030501 (R) (2013), URL https://link.aps.org/doi/10.1103/PhysRevA.87.030501.

[12] A. Wagner, S. Sturm, F. Köhler, D. A. Glazov, A. V. Volotka, G. Plunien, W. Quint, G. Werth, V. M. Shabaev, and K. Blaum, Phys. Rev. Lett. **110**, 033003 (2013), URL http://link.aps.org/doi/10.1103/PhysRevLett.110.033003.

[13] A. Gumberidze, T. Stöhlker, D. Banaś, K. Beckert, P. Beller, H. Beyer, F. Bosch, S. Hagmann, C. Kozhuharov, D. Liesen, et al., Phys. Rev. Lett. **94**, 223001 (2005), URL http://link.aps.org/doi/10.1103/PhysRevLett.94.223001.

[14] H. Bruhns, J. Braun, K. Kubiçek, J. R. Crespo López-Urrutia, and J. Ullrich, Phys. Rev. Lett. **99**, 113001 (2007), URL https://link.aps.org/doi/10.1103/PhysRevLett.99.113001.

[15] K. Kubiçek, P. H. Mokler, V. Mäckel, J. Ullrich, and J. R. Crespo López-Urrutia, Phys. Rev. A **90**, 032508 (2014), URL http://link.aps.org/doi/10.1103/PhysRevA.90.032508.

[16] V. A. Yerokhin and V. M. Shabaev, Journal of Physical and Chemical Reference Data **44**, 033103 (2015), URL http://scitation.aip.org/content/aip/journal/jpcrd/44/3/10.1063/1.4927487.

[17] S. W. Epp, R. Steinbrügge, S. Bernitt, J. K. Rudolph, C. Beilmann, H. Bekker, A. Müller, O. O. Versolato, H. C. Wille, H. Yavaş, et al., Phys. Rev. A **92**, 020502 (R) (2015), URL http://link.aps.org/doi/10.1103/PhysRevA.92.020502.

[18] P. Amaro, S. Schlesser, M. Guerra, E. O. Le Bigot, J.-M. Isac, P. Travers, J. P. Santos, C. I. Szabo, A. Gumberidze, and P. Indelicato, Phys. Rev. Lett. **109**, 043005 (2012), URL https://link.aps.org/doi/

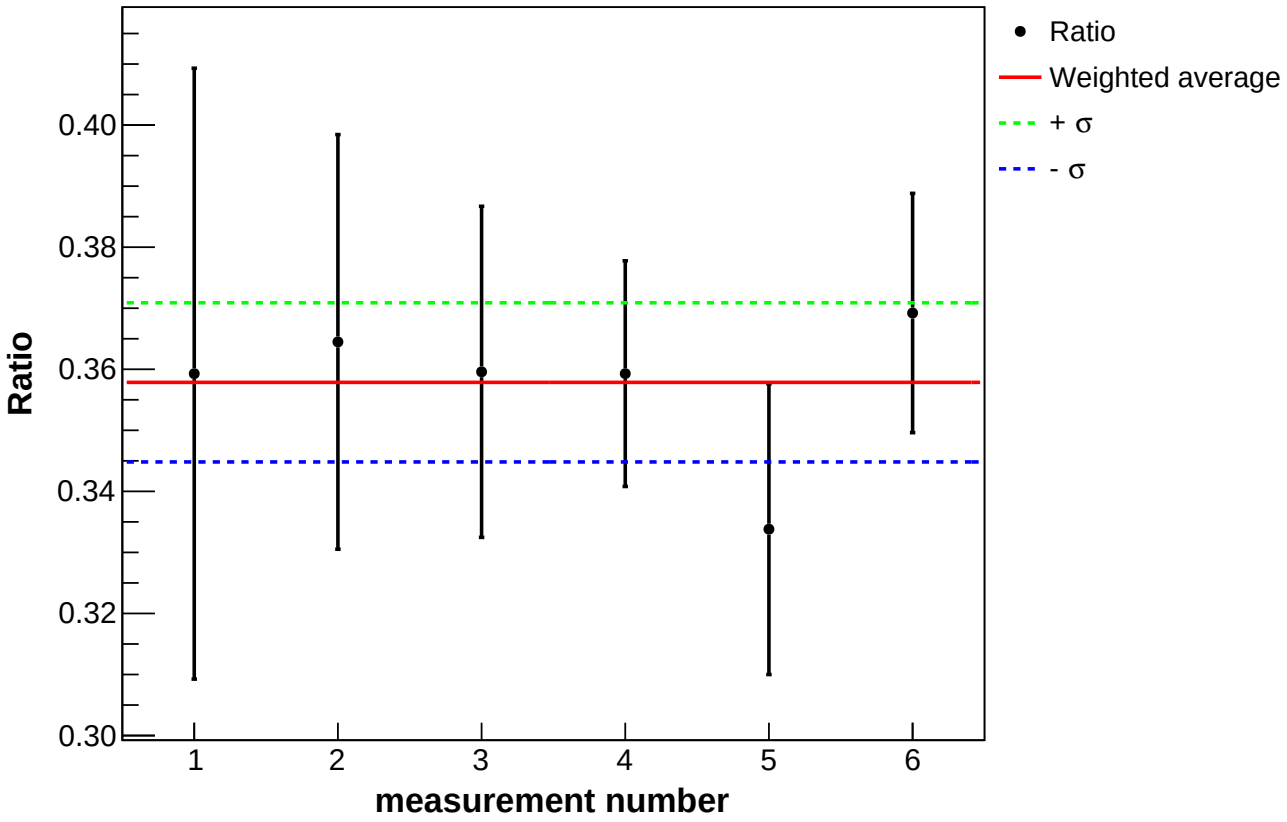


FIG. 18: (Color online) Ratio between the $1s\ 2s\ 2p\ ^2P_{1/2} \rightarrow 1s^2\ 2s\ ^2S_{1/2}$ and $1s\ 2s\ 2p\ ^2P_{3/2} \rightarrow 1s^2\ 2s\ ^2S_{1/2}$ transition intensities for all recorded dispersive spectra in argon. The weighted average value of 0.358 is represented by the solid red line and the $\pm\sigma = 0.013$ are represented by the green and blue dashed lines. The error bar at each point corresponds to the contribution of the uncertainty from the numerical integration of each peak.

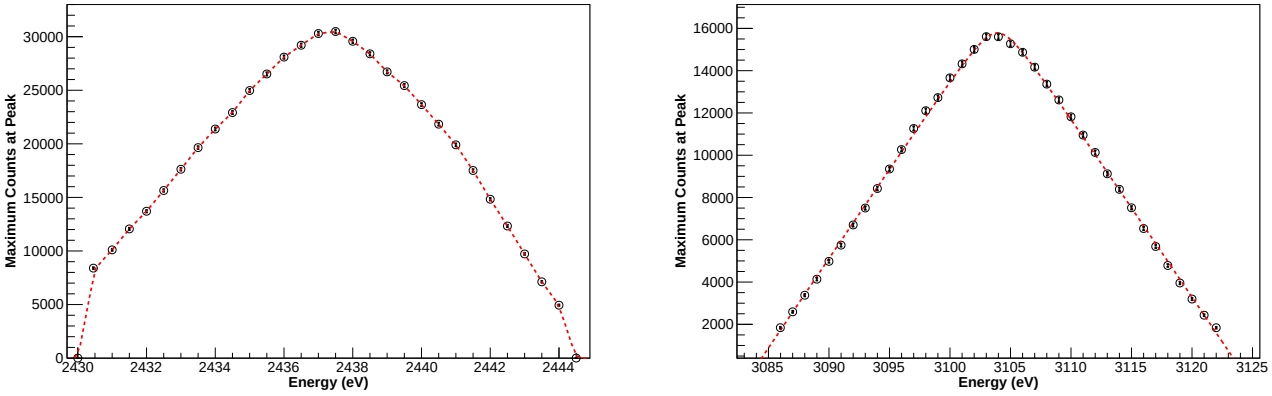


(a) Sulfur

(b) Argon

FIG. 19: (Color online) Transmitted intensity by the spectrometer for Li-like sulfur and argon as a function of x-ray energy following [125]. The red curve represents a fit with splines in sulfur and the fit with Eq. (9) in argon.

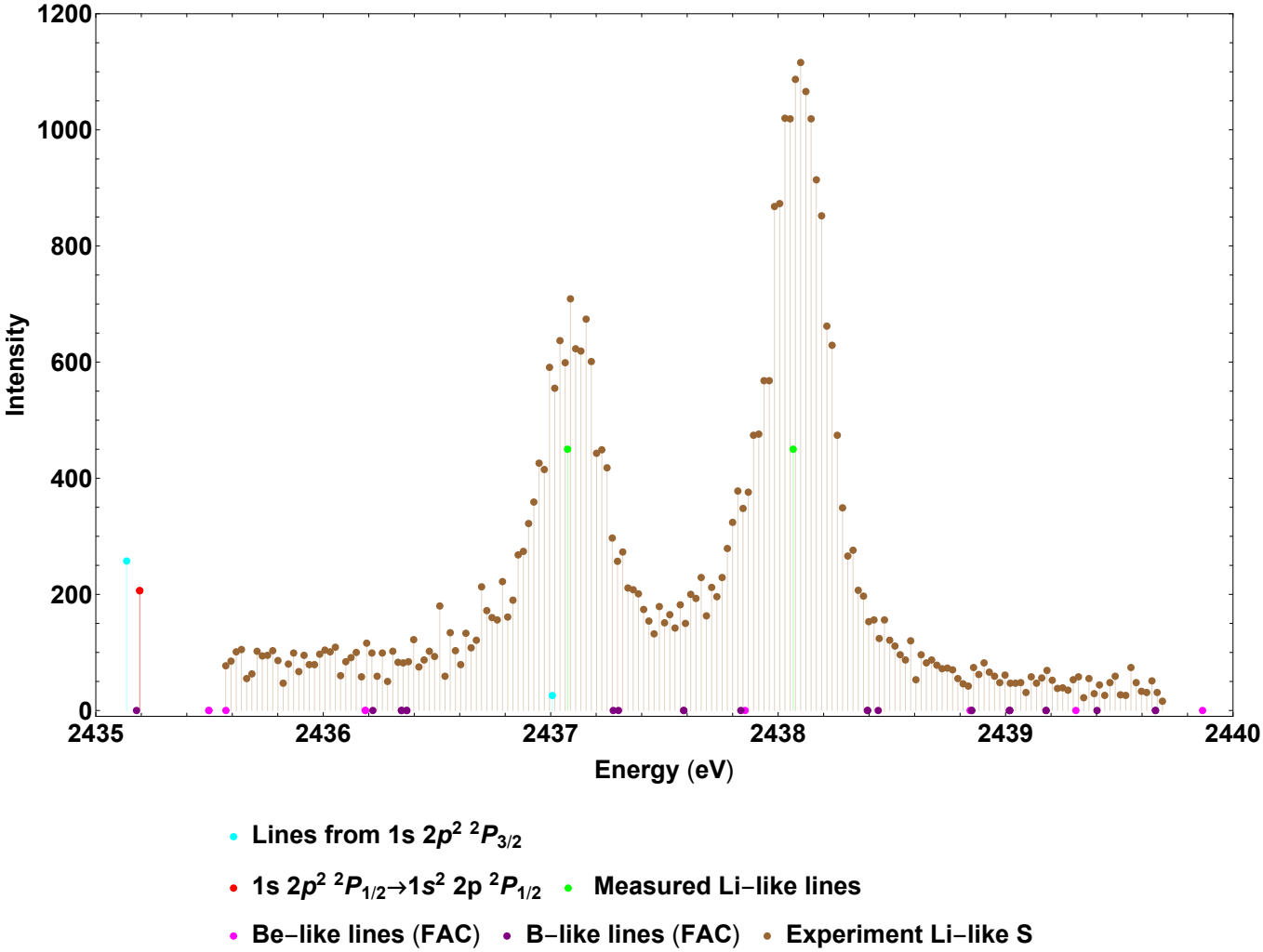


FIG. 20: (Color online) Possible blends to the $1s\ 2s\ 2p\ ^2P_{1/2} \rightarrow 1s^2\ 2s\ ^2S_{1/2}$ and $1s\ 2s\ 2p\ ^2P_{3/2} \rightarrow 1s^2\ 2s\ ^2S_{1/2}$ transitions in sulfur. The $1s\ 2p^2\ ^2P_{3/2} \rightarrow 1s^2\ 2p\ ^2P_{3/2}$, $1s\ 2p^2\ ^2P_{3/2} \rightarrow 1s^2\ 2p\ ^2P_{1/2}$ and the $1s\ 2p^2\ ^2P_{1/2} \rightarrow 1s^2\ 2p\ ^2P_{1/2}$ transition energies are from Ref. [32]. The relative intensities of the $1s\ 2p^2\ ^2P_{3/2} \rightarrow 1s^2\ 2p\ ^2P_{3/2}$ and $1s\ 2p^2\ ^2P_{3/2} \rightarrow 1s^2\ 2p\ ^2P_{1/2}$ transitions are evaluated using branching ratios calculated with FAC. The intensity of the $1s\ 2p^2\ ^2P_{1/2} \rightarrow 1s^2\ 2p\ ^2P_{1/2}$ transition is arbitrary, but it is the most intense of the doublet. The energies and relative intensities of the Be-like and B-like lines are evaluated using FAC. Their contributions are very small.

10.1103/PhysRevLett.109.043005.

[19] J. Machado, C. I. Szabo, J. P. Santos, P. Amaro, M. Guerra, A. Gumberidze, G. Bian, J. M. Isac, and P. Indelicato, Phys. Rev. A **97**, 032517 (2018), URL https://link.aps.org/doi/10.1103/PhysRevA.97.032517.

[20] A. N. Artemyev, V. M. Shabaev, V. A. Yerokhin, G. Plunien, and G. Soff, Phys. Rev. A **71**, 062104 (2005), URL http://link.aps.org/abstract/PRA/v71/e062104.

[21] J. Schweppe, A. Belkacem, L. Blumenfeld, N. Claytor, B. Feinberg, H. Gould, V. Kostroun, L. Levy, S. Misawa, R. Mowat, et al., Phys. Rev. Lett. **66**, 1434 (1991).

[22] C. Brandau, C. Kozhuharov, A. Müller, W. Shi, S. Schippers, T. Bartsch, S. Böhm, C. Böhme, A. Hoffknecht, H. Knopp, et al., Phys. Rev. Lett. **91**, 073202 (2003), URL http://link.aps.org/doi/10.1103/PhysRevLett.91.073202.

[23] P. Beiersdorfer, H. Chen, D. B. Thorn, and E. Träbert, Phys. Rev. Lett. **95**, 233003 (2005), URL http://link.aps.org/abstract/PRL/v95/e233003.

[24] P. Beiersdorfer, D. Knapp, R. E. Marrs, S. R. Elliot, and M. H. Chen, Phys. Rev. Lett. **71**, 3939 (1993).

[25] P. Beiersdorfer, A. Osterheld, S. R. Elliott, M. H. Chen, D. Knapp, and K. Reed, Phys. Rev. A **52**, 2693 (1995).

[26] P. Beiersdorfer, A. Osterheld, J. Scofield, J. R. Crespo López-Urrutia, and K. Widmann, Phys. Rev. Lett. **80**, 3022 (1998), URL http://journals.aps.org/prl/

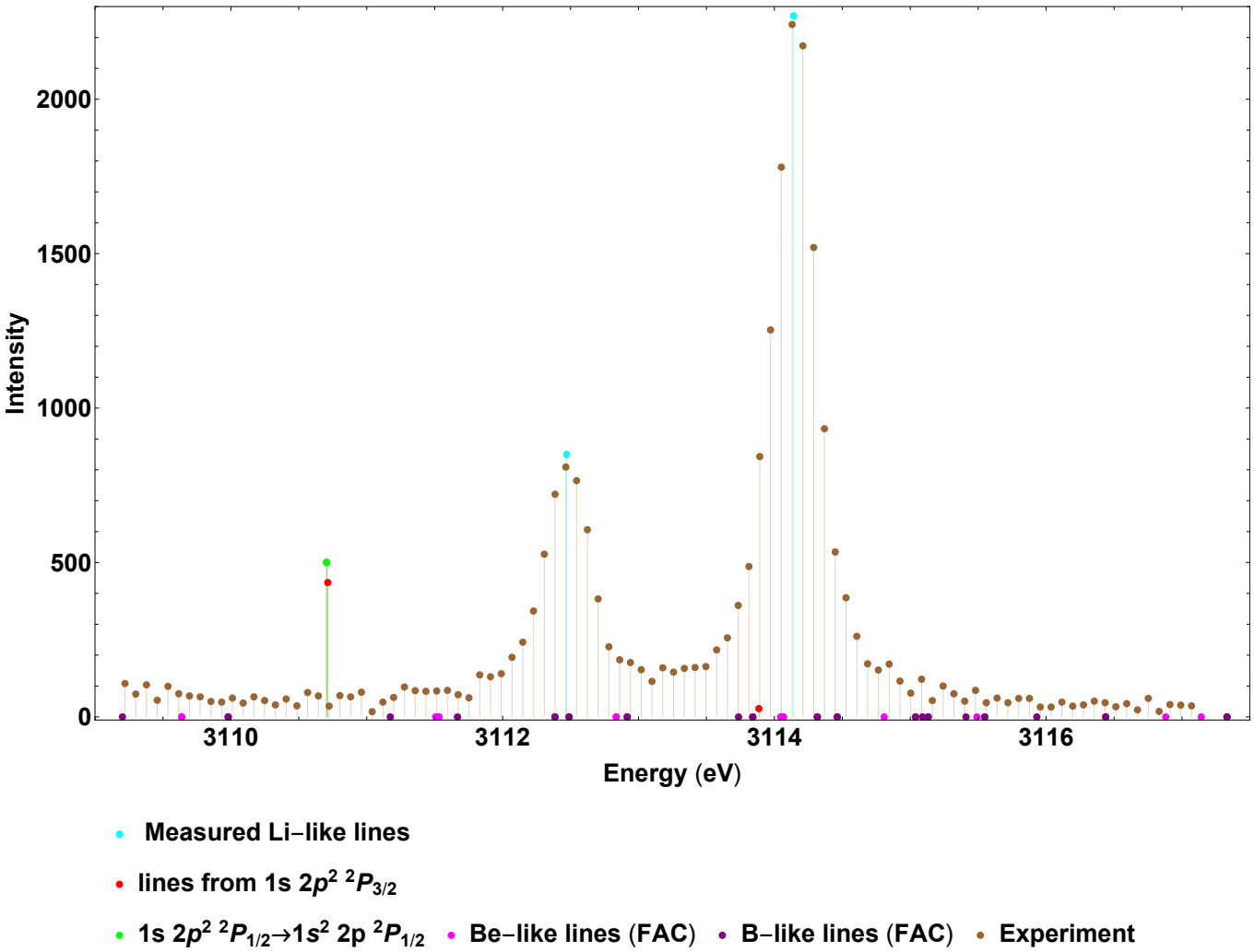


FIG. 21: (Color online) Possible blends to the $1s\ 2s\ 2p\ ^2P_{1/2} \rightarrow 1s^2\ 2s\ ^2S_{1/2}$ and $1s\ 2s\ 2p\ ^2P_{3/2} \rightarrow 1s^2\ 2s\ ^2S_{1/2}$ transitions in argon. The $1s\ 2p^2\ ^2P_{3/2} \rightarrow 1s^2\ 2p\ ^2P_{3/2}$, $1s\ 2p^2\ ^2P_{3/2} \rightarrow 1s^2\ 2p\ ^2P_{1/2}$ and the $1s\ 2p^2\ ^2P_{1/2} \rightarrow 1s^2\ 2p\ ^2P_{1/2}$ transition energies are from Ref. [31]. The relative intensities of the $1s\ 2p^2\ ^2P_{3/2} \rightarrow 1s^2\ 2p\ ^2P_{3/2}$ and $1s\ 2p^2\ ^2P_{3/2} \rightarrow 1s^2\ 2p\ ^2P_{1/2}$ transitions are evaluated using branching ratios calculated with FAC. The absence of a line at the expected position in the experimental spectrum shows that the contribution of this line to the intensity of the $1s\ 2s\ 2p\ ^2P_J \rightarrow 1s^2\ 2s\ ^2S_{1/2}$ doublet is negligible. The energies and relative intensities of the Be-like and B-like lines are also evaluated using FAC. Their contributions are very small.

abstract/10.1103/PhysRevLett.80.3022.

[27] X. Zhang, N. Nakamura, C. Chen, M. Andersson, Y. Liu, and S. Ohtani, Phys. Rev. A **78**, 032504 (2008), URL http://link.aps.org/abstract/PRA/v78/e032504http://dx.doi.org/10.1103/PhysRevA.78.032504.

[28] Y. Nakano, Y. Takano, T. Ikeda, Y. Kanai, S. Suda, T. Azuma, H. Bräuning, A. Bräuning-Demian, D. Dauvergne, T. Stöhlker, et al., Phys. Rev. A **87**, 060501 (R) (2013), URL http://link.aps.org/doi/10.1103/PhysRevA.87.060501.

[29] Y. S. Kozhedub, A. V. Volotka, A. N. Artemyev, D. A. Glazov, G. Plunien, V. M. Shabaev, I. I. Tupitsyn, and T. Stöhlker, Phys. Rev. A **81**, 042513 (2010), URL http://link.aps.org/doi/10.1103/PhysRevA.81.042513.

[30] J. Sapirstein and K. T. Cheng, Phys. Rev. A **83**, 012504 (2011), URL http://link.aps.org/doi/10.1103/PhysRevA.83.012504.

[31] V. A. Yerokhin and A. Surzhykov, Phys. Rev. A **86**, 042507 (2012), URL http://link.aps.org/doi/10.1103/PhysRevA.86.042507.

[32] V. A. Yerokhin, A. Surzhykov, and A. Müller, Phys. Rev. A **96**, 042505 (2017), URL https://link.aps.org/doi/10.1103/PhysRevA.96.042505.

[33] A. H. Gabriel, Monthly Notices of the Royal Astronomical Society **160**, 99 (1972), URL http://dx.doi.org/10.1093/mnras/160.1.99.

[34] E. V. Aglitskii, V. A. Boiko, S. M. Zakharov, S. A. Pikuz, and A. Y. Faenov, Soviet Journal of Quantum Electronics **4**, 500 (1974), URL http://stacks.iop.org/0049-1748/4/i=4/a=R16.

[35] E. Träbert, I. Armour, S. Bashkin, N. Jelley, R. O'Brien, and J. Silver, Journal of Physics B: Atomic, Molecular and Optical Physics **12**, 1665 (1979), URL http://iopscience.iop.org/article/10.1088/0022-3700/12/10/013.

[36] M. Bitter, K. W. Hill, M. Zarnstorff, S. von Goeler, R. Hulse, L. C. Johnson, N. R. Sauthoff, S. Sesnic, K. M. Young, M. Tavernier, et al., Phys. Rev. A **32**, 3011 (1985), URL http://link.aps.org/doi/10.1103/PhysRevA.32.3011.

[37] TFR Group, F. Bombarda, F. Bely-Dubau, P. Faucher, M. Cornille, J. Dubau, and M. Loulergue, Phys. Rev. A **32**, 2374 (1985), URL http://link.aps.org/doi/10.1103/PhysRevA.32.2374.

[38] TFR Group, M. Cornille, J. Dubau, and M. Loulergue, Phys. Rev. A **32**, 3000 (1985), URL https://link.aps.org/doi/10.1103/PhysRevA.32.3000.

[39] H. Hsuan, M. Bitter, K. W. Hills, S. von Goeler, B. Grek, D. Johnson, L. C. Johnson, S. Sesnic, C. P. Bhalla, K. R. Karim, et al., Phys. Rev. A **35**, 4280 (1987), URL http://journals.aps.org/pra/abstract/10.1103/PhysRevA.35.4280.

[40] P. Beiersdorfer, M. H. Chen, R. E. Marrs, M. B. Schneider, and R. S. Walling, Phys. Rev. A **44**, 396 (1991), URL http://link.aps.org/abstract/PRA/v44/p396.

[41] J. Suleiman, H. Berry, R. Dunford, R. Deslattes, and P. Indelicato, Phys. Rev. A **49**, 156 (1994), URL http://link.aps.org/doi/10.1103/PhysRevA.49.156.

[42] A. J. Smith, P. Beiersdorfer, V. Decaux, K. Widmann, A. Osterheld, and M. Chen, Phys. Rev. A **51**, 2808 (1995), URL http://link.aps.org/doi/10.1103/PhysRevA.51.2808.

[43] J. E. Rice, M. A. Graf, J. L. Terry, E. S. Marmar, K. Giesing, and F. Bombarda, J. Phys. B: At. Mol. Opt. Phys. **28**, 893 (1995), URL http://iopscience.iop.org/article/10.1088/0953-4075/28/5/021.

[44] V. Decaux, P. Beiersdorfer, S. M. Kahn, and V. L. Jacobs, The Astrophysical Journal **482**, 1076 (1997), URL http://stacks.iop.org/0004-637X/482/i=2/a=1076.

[45] B. J. Wargelin, S. M. Kahn, and P. Beiersdorfer, Phys. Rev. A **63**, 022710 (2001), URL https://link.aps.org/doi/10.1103/PhysRevA.63.022710.

[46] M. R. Tarbutt, R. Barnsley, N. J. Peacock, and J. D. Silver, J. Phys. B: At. Mol. Opt. Phys. **34**, 3979 (2001), URL http://stacks.iop.org/jb/34/3979.

[47] P. Beiersdorfer, M. Bitter, D. Hey, and K. J. Reed, Phys. Rev. A **66**, 032504 (2002), URL https://link.aps.org/doi/10.1103/PhysRevA.66.032504.

[48] V. Decaux, V. L. Jacobs, P. Beiersdorfer, D. A. Liedahl, and S. M. Kahn, Phys. Rev. A **68**, 012509 (2003), URL https://link.aps.org/doi/10.1103/PhysRevA.68.012509.

[49] C. Biedermann, R. Radtke, and K. Fournier, Nucl. Instr. Methods B **205**, 255 (2003), URL http://www.sciencedirect.com/science/article/pii/S0168583X02019730.

[50] J. K. Rudolph, S. Bernitt, S. W. Epp, R. Steinbrügge, C. Beilmann, G. V. Brown, S. Eberle, A. Graf, Z. Harman, N. Hell, et al., Phys. Rev. Lett. **111**, 103002 (2013), URL https://link.aps.org/doi/10.1103/PhysRevLett.111.103002.

[51] S. Schlesser, S. Boucard, D. S. Covita, J. M. F. dos Santos, H. Fuhrmann, D. Gotta, A. Gruber, M. Hennebach, A. Hirtl, P. Indelicato, et al., Phys. Rev. A **88**, 022503 (2013), URL http://link.aps.org/doi/10.1103/PhysRevA.88.022503.

[52] J. E. Rice, M. L. Reinke, J. M. A. Ashbourn, C. Gao, M. M. Victora, M. A. Chilenski, L. Delgado-Aparicio, N. T. Howard, A. E. Hubbard, J. W. Hughes, et al., J. Phys. B: At. Mol. Opt. Phys. **47**, 075701 (2014), URL http://stacks.iop.org/0953-4075/47/i=7/a=075701.

[53] D. B. Thorn, G. V. Brown, J. H. T. Clementson, H. Chen, M. Chen, P. Beiersdorfer, K. R. Boyce, C. A. Kilbourne, F. S. Porter, and R. L. Kelley, Can. J. Phys. **86**, 241 (2008), URL http://www.nrcresearchpress.com/doi/abs/10.1139/P07-134#.WY2cya1HmHo.

[54] H. D. Dohmann, D. Liesen, and H. Pfeng, Zeitschrift für Physik A Hadrons and Nuclei **285**, 171 (1978), URL http://dx.doi.org/10.1007/BF01408743.

[55] P. Indelicato and E. Lindroth, Phys. Rev. A **46**, 2426 (1992), URL https://journals.aps.org/pra/abstract/10.1103/PhysRevA.46.2426.

[56] T. Mooney, E. Lindroth, P. Indelicato, E. Kessler, and R. Deslattes, Phys. Rev. A **45**, 1531 (1992), URL http://link.aps.org/doi/10.1103/PhysRevA.45.1531.

[57] P. Indelicato, S. Boucard, and E. Lindroth, Eur. Phys. J. D **3**, 29 (1998), URL http://link.springer.com/article/10.1007/s100530050146.

[58] R. Deslattes, E. K. Jr., P. Indelicato, L. de Billy, E. Lindroth, and J. Anton, Rev. Mod. Phys. **75**, 35 (2003), URL http://www.physics.nist.gov/PhysRefData/XrayTrans/index.htmlhttp://link.aps.org/doi/10.1103/RevModPhys.75.35.

[59] P. Amaro, C. I. Szabo, S. Schlesser, A. Gumberidze, E. G. Kessler, A. Henins, E. O. Le Bigot, M. Trassinelli, J. M. Isac, P. Travers, et al., Radiat. Phys. and Chem. **98**, 132 (2014), URL http://linkinghub.elsevier.com/retrieve/pii/S0969806X1400019X.

[60] B. L. Henke, E. M. Gullikson, and J. C. Davis, At. Data Nucl. Data Tables **54**, 181 (1993), URL http://www.sciencedirect.com/science/article/B6WBB-45R7DJM-8/2/70158a249f3de7a951a3ae98a0b114ab.

[61] C. I. Szabo, P. Amaro, M. Guerra, S. Schlesser, A. Gumberidze, J. P. Santos, and P. Indelicato, in CAARI (AIP, Fort Worth, Texas, 2013), vol. 1525 of AIP Conference Proceedings, p. 68, URL http://stacks.iop.org/1402-4896/2013/i=T156/a=014077.

[62] C. I. Szabo, P. Amaro, M. Guerra, J. P. Santos, A. Gumberidze, J. Attard, and P. Indelicato, Phys. Scr. **2013**, 014077 (2013), URL http://stacks.iop.org/1402-4896/2013/i=T156/a=014077.

[63] W. H. Press, B. P. Flannery, S. A. Teukolsky, and W. T. Vetterling, Numerical Recipes 3rd Edition: The Art of Scientific Computing (Cambridge University Press, Cambridge, 2007).

[64] M. Trassinelli, Nucl. Instrum. Methods B **408**, 301 (2017), ISSN 0168-583X, URL https://www.sciencedirect.com/science/article/pii/S0168583X17306122.

[65] U. von Toussaint, Rev. Mod. Phys. **83**, 943 (2011), URL https://journals.aps.org/rmp/abstract/10.1103/RevModPhys.83.943.

[66] R. Trotta, Contemporary Physics **49**, 71 (2008), ISSN 0010-7514, URL https://www.tandfonline.com/doi/abs/10.1080/00107510802066753.

[67] D. S. Sivia and J. Skilling, Data analysis: a Bayesian tutorial (Oxford University Press, 2006), 2nd ed., ISBN 0198568320, 9780198568322.

[68] C. Gordon and R. Trotta, Monthly Notices of the Royal Astronomical Society **382**, 1859 (2007).

[69] J. P. Desclaux, Comp. Phys. Commun. **9**, 31 (1975), URL http://linkinghub.elsevier.com/retrieve/pii/0010465575900545.

[70] P. Indelicato and J. P. Desclaux, Phys. Rev. A **42**, 5139 (1990), URL http://journals.aps.org/pra/abstract/10.1103/PhysRevA.42.5139.

[71] P. Indelicato, O. Gorceix, and J. P. Desclaux, J. Phys. B: At. Mol. Opt. Phys. **20**, 651 (1987), URL http://dx.doi.org/10.1088/0022-3700/20/4/007.

[72] P. Indelicato and J. Desclaux, Mcdfgme, a multiconfiguration dirac fock and general matrix elements program (release 2005), URL http://kroll.lkb.upmc.fr/mcdf (2005).

[73] V. M. Shabaev, I. I. Tupitsyn, and V. A. Yerokhin, Phys. Rev. A **88**, 012513 (2013), URL http://link.aps.org/doi/10.1103/PhysRevA.88.012513.

[74] V. M. Shabaev, I. I. Tupitsyn, and V. A. Yerokhin, Comp. Phys. Commun. **189**, 175 (2015), URL http://www.sciencedirect.com/science/article/pii/S0010465514004081.

[75] V. A. Yerokhin, Phys. Rev. A **97**, 052509 (2018), URL https://link.aps.org/doi/10.1103/PhysRevA.97.052509.

[76] I. P. Grant, Advances in Physics **19**, 747 (1970), URL http://dx.doi.org/10.1080/00018737000101191.

[77] I. P. Grant and H. M. Quiney, Adv. At. Mol. Phys. **23**, 37 (1988), URL http://linkinghub.elsevier.com/retrieve/pii/S0065219908601050.

[78] P. Indelicato, Phys. Rev. A **51**, 1132 (1995), URL https://link.aps.org/doi/10.1103/PhysRevA.51.1132.

[79] V. M. Shabaev, Theoretical and Mathematical Physics **63**, 588 (1985), URL http://link.springer.com/10.1007/BF01017505.

[80] V. Shabaev and A. Artemyev, J. Phys. B: At. Mol. Opt. Phys. **27**, 1307 (1994), URL https://iopscience.iop.org/article/10.1088/0953-4075/27/7/006/meta.

[81] V. M. Shabaev, Phys. Rev. A **57**, 59 (1998), URL https://link.aps.org/doi/10.1103/PhysRevA.57.59.

[82] J. Li, C. Nazé, M. Godefroid, S. Fritzsche, G. Gaigalas, P. Indelicato, and P. Jönsson, Phys. Rev. A **86**, 022518 (2012), URL https://link.aps.org/doi/10.1103/PhysRevA.86.022518.

[83] J. M. Sampaio, F. Parente, C. Nazé, M. Godefroid, P. Indelicato, and J. P. Marques, Physica Scripta **2013**, 014015 (2013), URL http://stacks.iop.org/1402-4896/2013/i=T156/a=014015.

[84] G. Audi, A. H. Wapstra, and C. Thibault, Nucl. Phys. A **729**, 337 (2003), URL http://linkinghub.elsevier.com/retrieve/pii/S0375947403018098.

[85] I. Angeli, At. Data, Nucl. Data Tab. **87**, 185 (2004), URL http://linkinghub.elsevier.com/retrieve/pii/S0092640X04000166.

[86] I. Angeli and K. P. Marinova, At. Data Nucl. Data Tables **99**, 69 (2013), URL http://www.sciencedirect.com/science/article/pii/S0092640X12000265.

[87] J. P. Santos, J. P. Marques, F. Parente, E. Lindroth, P. Indelicato, and J. P. Desclaux, J. Phys. B: At. Mol. Phys. **32**, 2089 (1999), URL http://stacks.iop.org/0953-4075/32/i=9/a=304?key=crossref.acc554a6c6c41344197b09b5cb3520c9.

[88] J. P. Santos, G. C. Rodrigues, J. P. Marques, F. Parente, J. P. Desclaux, and P. Indelicato, Eur. Phys. J. D **37**, 201 (2006), URL http://www.springerlink.com/openurl.asp?genre=article&id=doi:10.1140/epjd/e2006-00002-x.

[89] M. C. Martins, J. P. Marques, A. M. Costa, J. P. Santos, F. Parente, S. Schlesser, E. O. Le Bigot, and P. Indelicato, Phys. Rev. A **80**, 032501 (2009), URL https://link.aps.org/doi/10.1103/PhysRevA.80.032501.

[90] P. Mohr, Annals of Physics **88**, 26 (1974), URL https://doi.org/10.1016/0003-4916(74)90398-4.

[91] P. J. Mohr, Phys. Rev. A **46**, 4421 (1992), URL https://link.aps.org/doi/10.1103/PhysRevA.46.4421.

[92] P. J. Mohr and Y.-K. Kim, Phys. Rev. A **45**, 2727 (1992), URL http://link.aps.org/doi/10.1103/PhysRevA.45.2727.

[93] P. Indelicato and P. J. Mohr, Phys. Rev. A **46**, 172 (1992), URL https://link.aps.org/doi/10.1103/PhysRevA.46.172.

[94] E.-O. Le Bigot, P. Indelicato, and P. J. Mohr, Phys. Rev. A **64**, 052508 (2001), URL https://link.aps.org/doi/10.1103/PhysRevA.64.052508.

[95] P. J. Mohr and G. Soff, Phys. Rev. Lett. **70**, 158 (1993), URL https://link.aps.org/doi/10.1103/PhysRevLett.70.158.

[96] P. Indelicato and P. J. Mohr, Hyp. Int. **114**, 147 (1998), URL http://link.springer.com/10.1023/A:1012622505367.

[97] V. Yerokhin, P. Indelicato, and V. Shabaev, Phys. Rev. Lett. **91**, 073001 (2003), URL http://journals.aps.org/prl/abstract/10.1103/PhysRevLett.91.073001.

[98] V. Yerokhin, P. Indelicato, and V. Shabaev, Eur. Phys. J. D **25**, 203 (2003), URL https://doi.org/10.1140/epjd/e2003-00270-x.

[99] V. A. Yerokhin, P. Indelicato, and V. M. Shabaev, Phys. Rev. Lett. **97**, 253004 (2006), URL http://link.aps.org/abstract/PRL/v97/e253004.

[100] V. A. Yerokhin, P. Indelicato, and V. M. Shabaev, Can. J. Phys. **85**, 521 (2007), URL http://dx.doi.org/10.1140/epjd/e2006-00064-8.

[101] V. A. Yerokhin, P. Indelicato, and V. M. Shabaev, Phys. Rev. A **77**, 062510 (2008).

[102] V. A. Yerokhin, Phys. Rev. A **80**, 040501 (R) (2009), URL http://link.aps.org/abstract/PRA/v80/e040501.

[103] V. A. Yerokhin, Eur. Phys. J. D **58**, 57 (2010), URL http://dx.doi.org/10.1140/epjd/e2010-00089-4.

[104] P. Indelicato, Phys. Rev. A **87**, 022501 (2013), URL http://link.aps.org/doi/10.1103/PhysRevA.87.022501.

[105] P. Indelicato, F. Parente, and R. Marrus, Phys. Rev. A **40**, 3505 (1989), URL https://link.aps.org/doi/10.1103/PhysRevA.40.3505.

[106] P.-O. Löwdin, Phys. Rev. **97**, 1474 (1955), URL https://link.aps.org/doi/10.1103/PhysRev.97.1471.

[107] P. Indelicato, Hyperfine Interaction **108**, 39 (1997), URL http://link.springer.com/10.1023/A:1012621620562.

[108] G. Howat, T. Åberg, and O. Goscinski, J. Phys. B: At. Mol. Opt. Phys. **11**, 1575 (1978), URL http://iopscience.iop.org/article/10.1088/0022-3700/11/9/011/meta.

[109] M. F. Gu, Can. J. Phys. **86**, 675 (2008), URL http://www.nrcresearchpress.com/doi/abs/10.1139/p07-197.

[110] F. F. Goryaev, L. A. Vainshtein, and A. M. Urnov, At. Data Nucl. Data Tables **113**, 117 (2017), URL http://www.sciencedirect.com/science/article/pii/S0092640X16300092.

[111] L. A. Vainshtein and U. I. Safronova, At. Data, Nucl. Data Tab. **21**, 49 (1978), URL http://www.sciencedirect.com/science/article/B6WBB-4DBJ1BP-4R/2/0d1af82df1b9a0cab467983280479be0.

[112] A. M. Costa, M. C. Martins, F. Parente, J. P. Santos, and P. Indelicato, At. Data, Nucl. Data Tab. **79**, 223 (2001), URL http://www.idealibrary.com/links/doi/10.1006/adnd.2001.0869.

[113] J. Nilsen, At. Data, Nucl. Data Tab. **38**, 339 (1988), URL http://www.sciencedirect.com/science/article/B6WBB-4DBJ6CP-44/2/b08d317acbf37d974f86941a43fb9bf4.

[114] C. P. Bhalla and T. W. Tunnell, Journal of Quantitative Spectroscopy and Radiative Transfer **32**, 141 (1984), URL http://www.sciencedirect.com/science/article/pii/0022407384900785.

[115] M. H. Chen, At. Data Nucl. Data Tables **34**, 301 (1986), URL http://www.sciencedirect.com/science/article/B6WBB-4DBJ104-1M/2/a8d72edf870f1ff9026aa7f9e28d3f36.

[116] A. D. Whiteford, N. R. Badnell, C. P. Ballance, S. D. Loch, M. G. O'Mullane, and H. P. Summers, Journal of Physics B: Atomic, Molecular and Optical Physics **35**, 3729 (2002), URL http://stacks.iop.org/0953-4075/35/i=17/a=309.

[117] U. I. Safronova and A. S. Shlyaptseva, Physica Scripta **54**, 254 (1996), URL http://stacks.iop.org/1402-4896/54/i=3/a=005.

[118] M. H. Chen, B. Crasemann, and H. Mark, Phys. Rev. A **24**, 1852 (1981), URL https://doi.org/10.1103/PhysRevA.24.1852.

[119] P. Indelicato and P. J. Mohr, Phys. Rev. A **63**, 052507 (2001), URL https://journals.aps.org/pra/abstract/10.1103/PhysRevA.63.052507.

[120] R. Brun and F. Rademakers, Nucl. Instr. Methods A **389**, 81 (1997), URL http://www.sciencedirect.com/science/article/pii/S016890029700048X.

[121] I. Antcheva, M. Ballintijn, B. Bellenot, M. Biskup, R. Brun, N. Buncic, P. Canal, D. Casadei, O. Couet, V. Fine, et al., Comp. Phys. Commun. **180**, 2499 (2009), URL http://www.sciencedirect.com/science/article/pii/S0010465509002550.

[122] I. Antcheva, M. Ballintijn, B. Bellenot, M. Biskup, R. Brun, N. Buncic, P. Canal, D. Casadei, O. Couet, V. Fine, et al., Comp. Phys. Commun. **182**, 1384 (2011), URL http://www.sciencedirect.com/science/article/pii/S0010465511000701.

[123] B. Gough, GNU Scientific Library Reference Manual - Third Editio (Network Theory Ltd., 2009), 3rd ed., ISBN 0954612078, 9780954612078.

[124] R. Piessens, E. de Doncker-Kapenga, C. W. Überhuber, and D. K. Kahaner, Quadpack: A Subroutine Package for Automatic Integration, Springer Series in Computational Mathematics (Springer Berlin Heidelberg, 2012).

[125] M. Guerra, P. Amaro, C. I. Szabo, A. Gumberidze, P. Indelicato, and J. P. Santos, J. Phys. B: At. Mol. Opt. Phys. **46**, 065701 (2013), URL http://stacks.iop.org/0953-4075/46/i=6/a=065701.